ARTICLE

doi:10.1038/nature17996

Midbrain circuits for defensive behaviour

Philip Tovote[1]*, Maria Soledad Esposito[1,2]*, Paolo Botta[1]†, Fabrice Chaudun[3], Jonathan P. Fadok[1], Milica Markovic[1], Steffen B. E. Wolff[1]†, Charu Ramakrishnan[4], Lief Fenno[4], Karl Deisseroth[4], Cyril Herry[3], Silvia Arber[1,2] & Andreas Lüthi[1]

Survival in threatening situations depends on the selection and rapid execution of an appropriate active or passive defensive response, yet the underlying brain circuitry is not understood. Here we use circuit-based optogenetic, *in vivo* and *in vitro* electrophysiological, and neuroanatomical tracing methods to define midbrain periaqueductal grey circuits for specific defensive behaviours. We identify an inhibitory pathway from the central nucleus of the amygdala to the ventrolateral periaqueductal grey that produces freezing by disinhibition of ventrolateral periaqueductal grey excitatory outputs to pre-motor targets in the magnocellular nucleus of the medulla. In addition, we provide evidence for anatomical and functional interaction of this freezing pathway with long-range and local circuits mediating flight. Our data define the neuronal circuitry underlying the execution of freezing, an evolutionarily conserved defensive behaviour, which is expressed by many species including fish, rodents and primates. In humans, dysregulation of this 'survival circuit' has been implicated in anxiety-related disorders.

Threatening situations, such as the presence of a predator or exposure to stimuli predicting imminent or perceived danger, evoke an evolutionarily conserved brain state, fear, which triggers defensive behaviours to avoid or reduce potential harm[1–3]. A long-standing question in fear and anxiety research has been how brain circuits generate various forms of defensive behaviours, which have been used as a read-out for normal fear and maladaptive anxiety[2,4–6]. In rodents, depending on threat imminence[7] and contextual factors such as the existence of escape routes, defensive behaviours range from risk assessment[8] and freezing[9,10] to flight and defensive attack[2,11]. These behaviours can be rapidly switched to adequately adapt to fluctuating threat levels or contextual challenges[11,12]. On the basis of electrical stimulation, lesion and pharmacological studies, the midbrain periaqueductal grey region (PAG) has been proposed to present an essential part of the circuitry that elicits freezing and flight in response to threat[12–22]. However, PAG circuit mechanisms underlying expression of defensive behaviours remain poorly understood. This includes a lack of knowledge about the functional roles of different PAG neuron types, their connectivity and regulation for expression of defensive behaviours. The PAG receives inputs from key forebrain regions involved in regulation of defensive behaviour, such as the central nucleus of the amygdala (CEA)[23,24], the hypothalamus[25–27] and medial prefrontal cortex[28], but little is known about their specific PAG cellular targets. In addition, the functional roles of long-range inputs to PAG, neuronal subpopulations within PAG subregions and intra-PAG microcircuitry, as well as outputs from PAG, in the expression of active and passive defensive behaviours is poorly understood. Using optogenetic manipulations of specific cell types, single-unit recordings and rabies-mediated neuroanatomical tracings, we here define a pathway from the CEA to the ventrolateral PAG (vlPAG) that mediates freezing by disinhibition of vlPAG outputs to pre-motor targets in the magnocellular nucleus (Mc) of the medulla. Furthermore, we provide evidence for anatomical and functional interaction of this 'freezing pathway' with circuits mediating flight.

Freezing is mediated by glutamatergic vlPAG neurons

To determine cellular diversity in the vlPAG that could be associated with a distinct behavioural phenotype, we used an optogenetic approach to specifically manipulate the activity of excitatory glutamatergic neurons, one of the main cell classes in the PAG. We targeted glutamatergic neurons expressing vesicular glutamate transporter 2 ($vGluT2^+$) by local injection of adeno-associated viruses (AAV) delivering a construct that contained a Cre-dependent channelrhodopsin-2 (ChR2) coupled to an mCherry tag into the vlPAG of *Vglut2-ires-Cre* mice (Fig. 1a, b and Extended Data Fig. 1a, b). Mice injected with AAVs containing a fluorescent tag only served as controls. We first optically manipulated cellular activity in naive mice under low-fear conditions (that is, at low freezing levels), during exposure to a novel context. Strikingly, light-activation of $vGluT2^+$ neurons of the vlPAG reliably triggered strong freezing behaviour during the 'light on' period (Fig. 1c and Supplementary Video 1), which was reflected by a marked decrease in behavioural activity (Fig. 1d). To define the endogenous function of vlPAG glutamatergic neurons, we next used viral-vector-mediated, Cre-dependent expression of archaerhodopsin (Arch) to optically inhibit these neurons (Fig. 1b and Extended Data Fig. 1c). Under low-fear conditions in naive mice, we did not observe an effect on freezing or behavioural activity (Fig. 1e, f). To investigate the necessity of vlPAG glutamatergic neurons for conditioned freezing behaviour, we subjected mice to auditory fear conditioning, followed by next-day re-exposure to an aversively conditioned tone stimulus (CS) or to the context previously paired with mild electrical foot-shocks. We found that optical inhibition of vlPAG $vGluT2^+$ neurons during the CS blocked tone-induced freezing (Fig. 1g and Supplementary Video 2). Similarly, freezing in the conditioning context was markedly reduced during optical inhibition of vlPAG $vGluT2^+$ neurons (Fig. 1h). These results demonstrate a role of vlPAG glutamatergic neurons in mediating conditioned freezing responses.

To determine whether these neurons serve a more general role in mediating freezing, we next tested the necessity of these neurons for producing freezing to an innate threat. Mice exhibit strong fear responses when exposed to large moving objects, probably because these resemble visual features of a natural predator[22,29]. We therefore exposed mice in an open-field arena to a remote controlled toy

[1]Friedrich Miescher Institute for Biomedical Research, Maulbeerstrasse 66, 4058 Basel, Switzerland. [2]Biozentrum, Department of Cell Biology, University of Basel, 4056 Basel, Switzerland. [3]INSERM, Neurocentre Magendie, U862, 146 Rue Léo-Saignat, Bordeaux 33077, France. [4]Stanford University, 318 Campus Drive West, Clark Center W080, Stanford, California 94305, USA. †Present addresses: Champalimaud Centre for the Unknown, Avenida de Brasilia, 1400-038 Lisbon, Portugal (P.B.); Center for Brain Science, Harvard University, Cambridge, Massachusetts 02138, USA (S.B.E.W.).
*These authors contributed equally to this work.

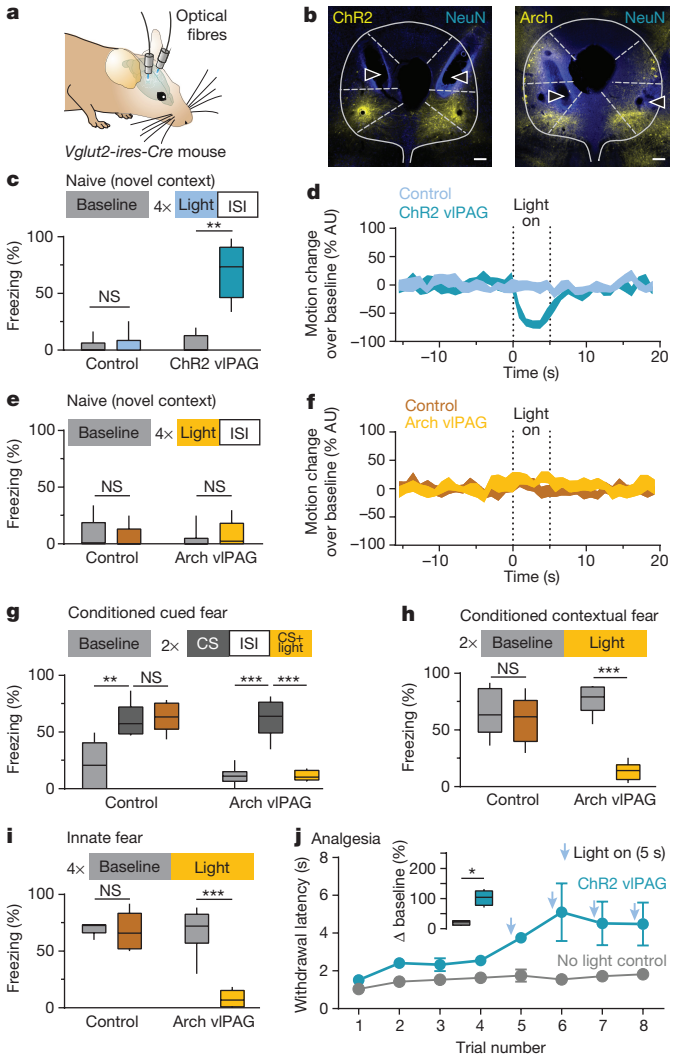

Figure 1 | Glutamatergic vlPAG neurons drive defensive responses. **a**, Optogenetics in freely moving mice. **b**, Expression patterns of ChR2 (left) and Arch (right) within vGluT2$^+$ vlPAG neurons (triangles, fibre tracts; scale bars, 200 μm). **c**, **d**, Light activation of glutamatergic vlPAG neurons triggered freezing behaviour ($n = 10$ ChR2, $n = 12$ control, two-tailed Wilcoxon signed-rank test). **e**, **f**, Inhibition of vlPAG glutamatergic neurons had no effect on freezing or behavioural activity in naive mice ($n = 7$ Arch, $n = 12$ control, two-tailed Wilcoxon signed-rank test). **g**–**i**, Inhibition of vlPAG glutamatergic neurons diminished CS-induced freezing ($n = 6$ per group, 1×3 analysis of variance (ANOVA), $F_{(2,10)} = 37.72$, $P < 0.001$, Tukey's post-hoc test), contextual freezing ($n = 6$ Arch, $n = 8$ control, paired two-tailed Student's t-test) and innate freezing responses ($n = 6$ Arch, $n = 5$ control, paired two-tailed Student's t-test). **j**, Light activation of vlPAG glutamatergic neurons induced analgesia ($n = 6$ ChR2, $n = 10$ control, unpaired two-tailed Student's t-test). Box–whisker plots indicate median, interquartile range and 5th–95th percentiles of the distribution. Motion plots depict s.e.m. range. $^*P < 0.05$; $^{**}P < 0.01$; $^{***}P < 0.001$.

snake (Extended Data Fig. 1d). We found that while mice exhibited strong freezing responses in the presence of the fear stimulus, this reaction was dramatically reduced by yellow-light-mediated inhibition of vlPAG vGluT2$^+$ neurons (Fig. 1i and Extended Data Fig. 1e). The reduction in freezing was attributable to optical inhibition and not to changes in threat imminence as measured by spatial distance between mouse and snake (Extended Data Fig. 1f, h). Taken together, these findings demonstrate that activation of vlPAG glutamatergic neurons is necessary for both learned and innate freezing, and that it can generate freezing in the absence of threat.

Because the PAG is involved in processing ascending and descending pain information from the periphery[30–32], it is conceivable that the observed behavioural responses were related to enhanced light-evoked pain perception. However, when we tested nociception using a tail immersion test, we found that optical activation of vGluT2$^+$ vlPAG neurons had a marked analgesic effect (Fig. 1j). These experiments identify a cellular substrate in the vlPAG for analgesia, an important part of the defensive response to threat.

A disinhibitory pathway from CEA to vlPAG

To address the question of how vlPAG vGluT2$^+$ neurons are regulated, we first aimed to characterize inputs to the vlPAG from the CEA, because of their suggested major roles in the expression of freezing[5,12,33,34]. To identify the CEA neurons contacting vlPAG, we injected retrogradely transported red fluorescent latex beads into the vlPAG of a reporter mouse strain, in which GABAergic (γ-aminobutyric-acid-releasing) cells express enhanced green fluorescent protein (*Gad1–eGFP*; Fig. 2a). Retrogradely transported beads were found throughout the CEA (Fig. 2a). Quantification of overlap between beads and GFP$^+$ neurons (Fig. 2b) showed that the CEA sends a GABAergic projection to vlPAG, consistent with previous reports[24]. Freezing is elicited through enhanced CEA output[33,35], but since these neurons are GABAergic, this would result in enhanced inhibition of their vlPAG targets. However, our results from optogenetic manipulation of freezing behaviour suggest that freezing is associated with increased activity of vlPAG glutamatergic neurons. Thus, the most parsimonious explanation consistent with these observations would involve a local vlPAG disinhibitory circuit mechanism that could convert an inhibitory input from CEA into enhanced output of vlPAG glutamatergic neurons.

To test this hypothesis, we traced monosynaptic connections of CEA cells onto either glutamatergic or GABAergic cells in the vlPAG (Fig. 2c) using Cre-dependent, cell-type-specific infection with pseudotyped EnvA-G-deleted rabies virus (EnvA-ΔG-rabies)[36] in *Vglut2-ires-Cre* or *Gad2-ires-Cre* mouse lines. These experiments revealed that CEA projections preferentially target vlPAG GABAergic cells (Fig. 2d, e). Complementing evidence for a disinhibitory CEA–vlPAG circuit was provided by whole-cell patch-clamp recordings of vlPAG GABAergic cells during optical activation of CEA terminals in acute brainstem slices containing PAG (Extended Data Fig. 2a). This experiment confirmed the existence of such inhibitory connections to vlPAG GABAergic neurons (Extended Data Fig. 2b–f and Fig. 2f). We also probed the existence of functional connections between local GABAergic and glutamatergic cells in the vlPAG. Glutamatergic cells were visualized by viral-vector-mediated, Cre-dependent expression of tdTomato in the vlPAG of *Vglut2-ires-Cre* mice (Fig. 2g). Using a double-conditional viral approach[37], ChR2 was introduced into vlPAG of non-vGluT2$^+$ cells. We recorded from identified vGluT2$^+$ neurons in acute brain slices during optical activation of local, non-vGluT2$^+$ neurons (Fig. 2h). In 50% of all recorded vGluT2$^+$ cells, we observed optically evoked inhibitory postsynaptic potentials (eIPSCs; average latency = 5.5 ms) (Fig. 2i) that were completely blocked by application of picrotoxin, a $GABA_A$ receptor antagonist (Fig. 2i, j). Taken together, our data from slice recordings and tracing experiments suggest that freezing is caused by a disinhibitory process within vlPAG that involves CEA-mediated inhibition of local GABAergic neurons resulting in enhanced activity of glutamatergic vlPAG neurons (Fig. 2f).

Local vlPAG GABAergic neurons control freezing

To investigate whether *in vivo* neuronal correlates of freezing in the vlPAG would be consistent with a disinhibitory circuit mechanism, we next performed single-unit recordings within vlPAG in freely moving mice (Fig. 3a). Mice with chronically implanted recording electrodes (Fig. 3b and Extended Data Fig. 3a) were fear conditioned and freezing responses were evoked during a fear retrieval session 24 h

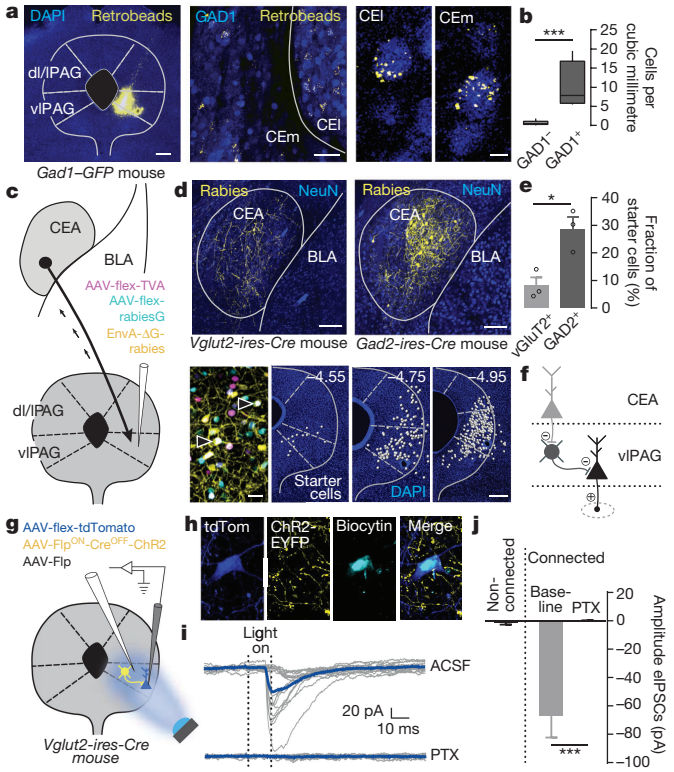

Figure 2 | A disinhibitory pathway from CEA to vlPAG. a, Fluorescent latex beads in vlPAG (left, scale bar, 200 μm). Beads were found in medial (CEm) and lateral (CEl) CEA cells (middle, scale bar, 40 μm; zoom-in shown in two right panels, scale bar, 5 μm). **b**, Overlap between beads and GAD1^{+} or GAD1^{-} neurons ($n = 2$ mice, two-tailed Mann–Whitney test). **c**, Cell-type-specific monosynaptic rabies tracing strategy. **d**, Rabies-labelled cells within CEA of *Vglut2-Cre* or *GAD2-Cre* mice (top panels, scale bar, 100 μm). Starter cells coexpressing TVA–GFP, rabiesG-V5 and EnvA-ΔG–mCherry–rabies (black triangles, bottom left panel, scale bar, 25 μm). Example of starter cells (white dots, three bottom right panels; numbers indicate distance from bregma; scale bar, 200 μm). **e**, Normalized number of rabies cells in CEA ($n = 3$ *Vglut2-Cre* mice, $n = 3$ *GAD2-Cre* mice, unpaired two-tailed Student's *t*-test). **f**, Schematic model of a disinhibitory pathway from CEA to vlPAG. **g**, **h**, Expression of ChR2 in non-glutamatergic neurons and tdTomato in glutamatergic neurons for targeted whole-cell patch-clamp recordings (scale bar, 10 μm). **i**, **j**, Light-evoked IPSCs (observed in 50% of all glutamatergic neurons tested) were blocked by PTX application ($n = 12$ cells from six slices of four mice, two-tailed 1 × 3 ANOVA, $F_{(2,15)} = 18.88$, $P < 0.0001$, Sidak's post-hoc test). Box–whisker plots indicate median, interquartile range and 5th–95th percentiles of the distribution; bar plots indicate mean ± s.e.m. $^{*}P < 0.05$, $^{***}P < 0.001$.

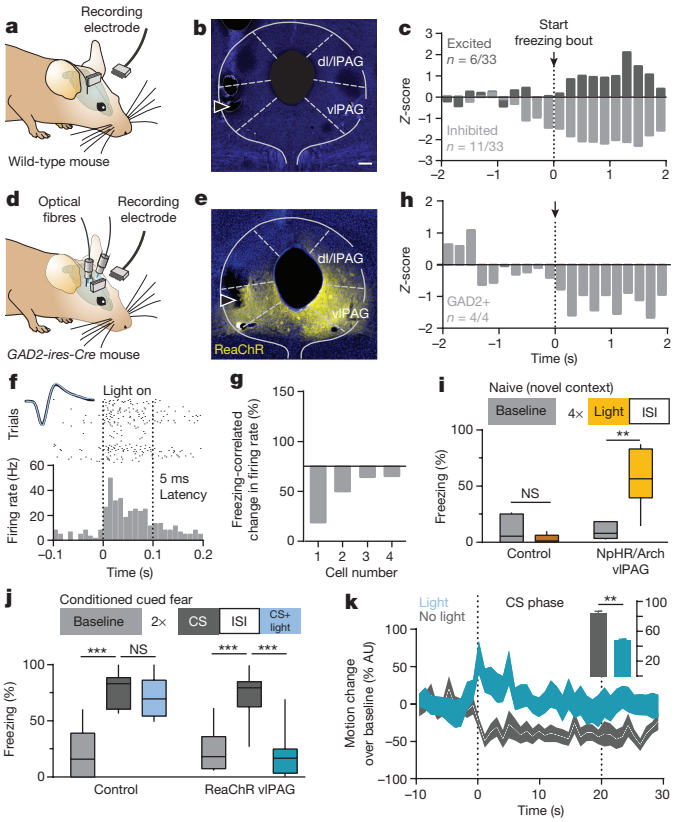

Figure 3 | GABAergic vlPAG neurons control freezing. a, Single-unit recordings in the vlPAG of freely moving wild-type mice. **b**, Example of a recording site (triangle; scale bar, 200 μm). **c**, vlPAG neuronal populations showing increased or decreased activity during freezing ($n = 8$ mice; bin size, 10 ms). **d**, Optical identification of GAD2^{+} single units in the vlPAG. **e**, Example of ChR2 expression and recording site (triangle; scale bar, 200 μm). **f**, Identified GAD2^{+} neuron activated by light with short latency (5 ms; bin size, 10 ms). Inset: mean spontaneous and light-evoked spike waveform. **g**, **h**, GAD2^{+} neurons exhibited reduced firing rates during freezing (four cells from three mice). **i**, Optical inhibition of GAD2^{+} neurons induced freezing in naive mice ($n = 6$ per group, two-tailed paired Student's *t*-test). **j**, **k**, Optical activation of GAD2^{+} neurons impaired CS-evoked freezing ($n = 12$ per group, two-tailed Friedman test, $P < 0.0001$, Dunn's multiple comparison test), and shifted CS-induced fear responses towards active behaviour ($n = 12$ per group, two-tailed paired Student's *t*-test). Box–whisker plots indicate median, interquartile range, and 5th–95th percentiles of the distribution; bars indicate mean ± s.e.m. Motion plots depict s.e.m. range. $^{*}P < 0.05$, $^{**}P < 0.01$, $^{***}P < 0.001$.

later[38]. Principal component analysis of single-unit activity in relation to freezing behaviour revealed that while one population of neurons (18%) was activated during freezing bouts, another population (33%) was inhibited (Fig. 3c). Consequently, we examined whether glutamatergic and GABAergic neurons could contribute to these differential activity patterns. To address this question, we performed recordings from optogenetically identified[39] GAD2^{+} and vGluT2^{+} neurons within vlPAG (Fig. 3d–f and Extended Data Fig. 3b). In agreement with a disinhibitory vlPAG freezing circuit, light-identified GAD2^{+} neurons ($n = 4$; Fig. 3g) exhibited a relatively high median baseline firing rate (8.3 Hz), and all showed lower firing rates during freezing compared with non-freezing periods (Fig. 3g, h). Recordings from identified vGluT2^{+} units ($n = 6$, median baseline firing rate = 3.0 Hz; Extended Data Fig. 3c–e) during freezing periods revealed a more heterogeneous picture, suggesting the existence of multiple subpopulations of glutamatergic neurons in vlPAG. Thus, the *in vivo* correlates of freezing are consistent with a disinhibitory circuit design leading to the activation of a subpopulation of glutamatergic vlPAG neurons during freezing.

An important prediction of this model is that manipulating the activity of GABAergic vlPAG neurons should affect freezing. In line with this interpretation, optogenetic inhibition of vlPAG GAD2^{+} neurons resulted in markedly enhanced freezing levels in naive animals (Fig. 3i and Extended Data Fig. 3f). Importantly, activation of GAD2^{+} neurons reduced freezing in response to a conditioned tone (Fig. 3j and Extended Data Fig. 3g). Moreover, this manipulation not only reduced CS-induced freezing but also resulted in transiently enhanced locomotor activity, resembling flight responses (Fig. 3k). Freezing was also reduced by optical activation of GAD2^{+} neurons during re-exposure to the conditioning context (Extended Data Fig. 3h), as well as in the presence of an unconditioned threatening stimulus (Extended Data Fig. 3i), while it had no effect on freezing in low-fear conditions (a novel context; Extended Data Fig. 3j). Taken together, these data are fully compatible with a circuit organization wherein inhibition of

local GABAergic vlPAG neurons leads to activation of glutamatergic neurons that is both necessary and sufficient to induce freezing behaviour.

vlPAG output to Mc drives freezing

We next sought to identify the output pathway mediating the freezing response. Analysis of axonal projections and synaptic boutons of vGluT2$^+$ vlPAG neurons (Extended Data Fig. 4a) showed that medullary regions previously implicated in motor control, such as the Mc[40,41], were a major synaptic target. To determine whether vGluT2$^+$ vlPAG neurons target pre-motor neurons in the Mc directly, we performed monosynaptic rabies tracing from forelimb motor neurons in adult *Chat-ires-Cre* mice (Fig. 4a). We visualized glutamatergic vlPAG terminals by unconditional viral expression of the presynaptic marker synaptophysin–GFP (Syn–GFP; Extended Data Fig. 4b) with synaptic co-localization of vGluT2 (Fig. 4b). Analysis of presynaptic inputs to forelimb pre-motor Mc neurons revealed that they were directly contacted by glutamatergic vlPAG neurons (Fig. 4c and Extended Data Fig. 4c–e).

We then asked whether vlPAG Mc-projecting glutamatergic neurons receive local inhibitory input. We first used a monosynaptic intersectional rabies tracing approach to specifically label presynaptic neurons in the vlPAG projecting onto glutamatergic neurons which target Mc (Extended Data Fig. 4f). We found that one-third of the local presynaptic neurons were GAD1$^+$ (Extended Data Fig. 4g, h), and thus putative sources of GABAergic inhibition onto glutamatergic vlPAG output cells. Furthermore, we probed the existence of functional connections between local GABAergic and Mc-projecting glutamatergic vlPAG cells by combining the approach described in Fig. 2g with an injection of retrogradely transported latex beads into the Mc (Fig. 4d). All Mc-projecting vGluT2$^+$ neurons recorded in whole-cell patch-clamp showed eIPSCs induced by light activation of vlPAG non-vGluT2$^+$ cells, which were blocked by picrotoxin application (Fig. 4e). These findings provide evidence that excitatory vlPAG output to the Mc is under local GABAergic control and suggest that this pathway could be part of the disinhibitory circuit underlying freezing.

To establish functional relevance of this projection for the freezing response, we next used an intersectional optogenetic approach to specifically manipulate activity of the glutamatergic vlPAG-to-Mc projection. We injected into the Mc of *Vglut2-ires-Cre* mice retrogradely trafficked herpes simplex virus (HSV), which Cre-dependently expresses flipase (Flp)[42]. This allowed us to selectively introduce ChR2 into vlPAG glutamatergic neurons projecting to Mc (vlPAG-to-Mc) on the basis of their co-expression of both Cre and Flp using double conditional AAVs (Fig. 4f and Extended Data Fig. 4i–k). Optical activation of glutamatergic vlPAG-to-Mc neurons resulted in instantaneous and strong freezing behaviour as reflected by decreased behavioural activity (Fig. 4g, h, Extended Data Fig. 4l and Supplementary Video 3). Interestingly, and in contrast to the anti-nociceptive effect elicited upon projection-unspecific activation of vGluT2$^+$ neurons in the vlPAG (Fig. 1j), no analgesia was observed after stimulation of the glutamatergic vlPAG-to-Mc neurons (Fig. 4i). Together, these findings demonstrate that vlPAG-to-Mc glutamatergic projection neurons are specifically involved in the expression of freezing behaviour and suggest that analgesia and freezing could be mediated by distinct subpopulations of vlPAG glutamatergic neurons.

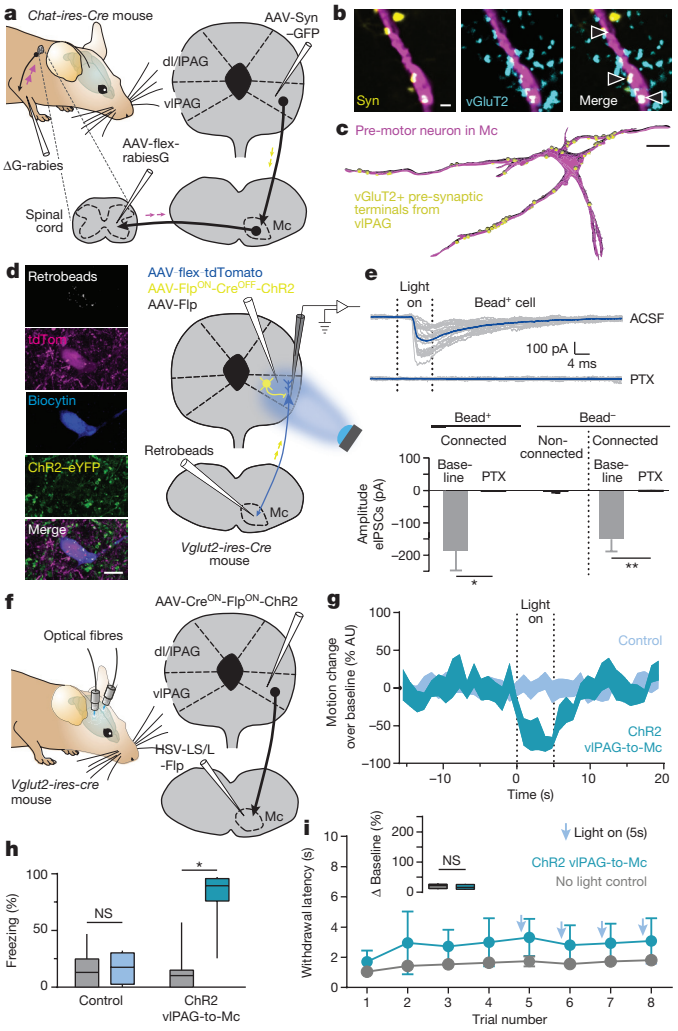

Figure 4 | Glutamatergic output to the Mc drives freezing. a, Strategy to assess vlPAG input onto Mc pre-motor neurons. **b**, vlPAG glutamatergic synapses contacting Mc pre-motor neurons were identified by co-staining of Syn–GFP and vGlut2 (triangles; scale bar, 2 μm). **c**, Three-dimensional reconstruction of a Mc pre-motor neuron contacted by vlPAG vGluT2$^+$ synapses (yellow circles; scale bar, 10 μm). **d**, Intersectional approach to investigate connectivity of vlPAG GABAergic cells with Mc-projecting glutamatergic neurons. **e**, Light activation of non-glutamatergic fibres evoked IPSCs in all bead$^+$ Mc-projecting glutamatergic neurons tested (nine out of nine cells, one example cell shown), and six out of nine glutamatergic, bead$^-$ neurons. All eIPSCs were blocked by PTX application (four slices of four mice; bead$^+$: two-tailed Wilcoxon signed-rank test; bead$^-$: 1×3 ANOVA $F_{(2,10)} = 10.28$, $P < 0.01$, Sidak's post-hoc test). **f**, Strategy to express ChR2 selectively in glutamatergic vlPAG neurons projecting to Mc. **g**, **h**, Light activation of glutamatergic vlPAG neurons projecting to Mc in naive mice resulted in strong freezing ($n = 7$ ChR2, $n = 10$ control, two-tailed Wilcoxon signed-rank test). **i**, Light activation of the glutamatergic vlPAG-to-Mc projection had no effect on nociception ($n = 5$ ChR2, $n = 11$ control, unpaired two-tailed Student's t-test). Box–whisker plots indicate median, interquartile range and 5th–95th percentiles of the distribution; bar plots indicate mean ± s.e.m. Motion plots depict s.e.m. range. $^*P < 0.05$; $^{**}P < 0.01$.

Interactions between freezing and flight pathways

Our data show that activation of vlPAG vGluT2$^+$ neurons induces freezing (Fig. 1). However, in mice with viral expression extending to dl/lPAG, we observed radically different, active defensive behavioural responses through optical activation of vGluT2$^+$ neurons (Fig. 5a and Extended Data Fig. 5a). These consisted of strong light-induced locomotor activity (Fig. 5b), amounting to marked flight responses in some cases. Nonetheless, bouts of forward locomotor activity were often interrupted by short periods of freezing, which resulted, on average, in intermediate levels of freezing (Fig. 5c and Extended Data Fig. 5b). Broad activation of vGluT2$^+$ neurons within PAG also resulted in strong analgesia (Fig. 5d). Given the observation of alternating active and passive defensive responses, this strongly suggests intricate interactions between flight and freezing circuits and raises

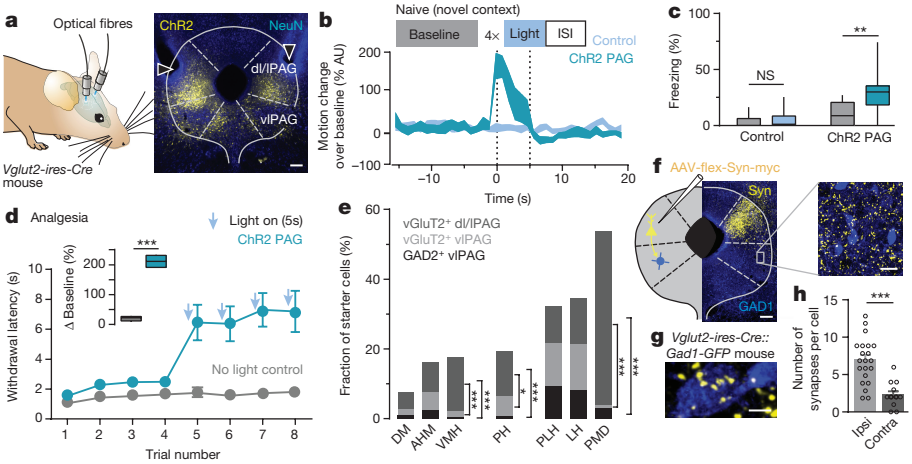

Figure 5 | Interactions between PAG freezing and flight pathways. **a**, Optogenetic manipulation of vGluT2$^+$ neurons in dl/lPAG and vlPAG (triangles indicate fibre tracts; scale bar, 200 μm). **b**, **c**, Light activation of PAG glutamatergic neurons in naive mice resulted in flight responses and intermediate freezing levels ($n = 12$ ChR2, $n = 12$ control, two-tailed Wilcoxon signed-rank test). **d**, Light activation of PAG glutamatergic neurons resulted in strong analgesia ($n = 9$ ChR2, $n = 10$ control, unpaired two-tailed Student's *t*-test). **e**, Hypothalamic presynaptic inputs onto vGluT2$^+$ ($n = 3$ mice for each vlPAG and dl/lPAG) and GAD2$^+$ ($n = 4$ mice) neurons within vlPAG or dl/lPAG (1×3 ANOVA, Tukey's post-hoc test for each analysed region). Quantification reveals differential input of hypothalamic subregions to vGluT2$^+$ ($n = 3$ mice for each vlPAG and dl/lPAG) and GAD2$^+$ ($n = 4$ mice) neurons within vlPAG or dl/lPAG. Ventromedial hypothalamic nucleus (VMH) (1×3 ANOVA, $F_{(2,7)} = 40.22$, $P < 0.0001$, Tukey's post-hoc test), posterior hypothalamic nucleus (PH) (1×3 ANOVA, $F_{(2,7)} = 21.01$, $P < 0.05$, Tukey's post-hoc test) and premammillary nucleus (PMD) (1×3 ANOVA, $F_{(2,7)} = 287$, $P < 0.0001$, Tukey's post-hoc test) preferentially target dl/lPAG vGluT2$^+$ neurons, whereas dorsomedial hypothalamic nucleus (DM) (1×3 ANOVA, $F_{(2,7)} = 4.082$, $P > 0.05$), anterior hypothalamus, medial part (AHM) (1×3 ANOVA, $F_{(2,7)} = 3.294$, $P > 0.05$), peduncular part of lateral hypothalamus (PLH) (1×3 ANOVA, $F_{(2,7)} = 0.153$, $P > 0.05$) and lateral hypothalamic area (LH) (1×3 ANOVA, $F_{(2,7)} = 0.948$, $P > 0.05$) showed no preference. **f**, Expression of Syn-myc in glutamatergic terminals of dl/lPAG projections to GABAergic neurons within vlPAG (left scale bar, 200 μm; right scale bar, 20 μm). **g**, High-resolution image of a GAD1$^+$ vlPAG neuron with dl/lPAG input (scale bar, 5 μm). **h**, Quantification of dl/lPAG vGluT2$^+$ synapses onto vlPAG GAD1$^+$ ($n = 21$ ipsilateral cells from four mice, $n = 13$ contralateral cells from two mice, unpaired two-tailed Student's *t*-test). Box–whisker plots indicate median, interquartile range and 5th–95th percentiles of the distribution; bar plots indicate mean ± s.e.m.; motion plots depict s.e.m. $^*P < 0.05$; $^{***}P < 0.001$.

the question of how such interactions are implemented within PAG circuitry.

We therefore examined whether distinct presynaptic inputs differentially connect onto specific PAG neuronal subpopulations (Extended Data Fig. 5c). Monosynaptic, cell-specific rabies tracing revealed high selectivity in the hypothalamic projections to defined PAG neuronal subpopulations (Fig. 5e and Extended Data Fig. 5d–f). It is conceivable that hypothalamic input to both dl/lPAG and vlPAG glutamatergic neurons promotes a range of defensive behaviours[26,27]. In turn, activity of the disinhibitory pathway originating in the CEA might bias the behavioural response towards freezing instead of flight. We thus hypothesized that, because of their role in controlling freezing, GABAergic neurons of the vlPAG are poised to present a neuronal substrate for the interaction of freezing and flight pathways. Consequently, we asked whether glutamatergic, flight-promoting neurons of the dl/lPAG could negatively regulate vlPAG excitatory output via activation of vlPAG GABAergic neurons to inhibit the freezing response. In offspring of *Vglut2-ires-Cre* crossed with *Gad1–eGFP* mice, we performed minimal injections of diluted virus to Cre-dependently express Syn-Myc in vGluT2$^+$ dl/lPAG neurons only (Fig. 5f). In line with our hypothesis, we found that dl/lPAG glutamatergic neurons form synaptic contacts with GABAergic vlPAG cells (Fig. 5g, h), whose optical activation can lead to flight responses (Fig. 3k). These results support the notion that vlPAG GABAergic neurons integrate multiple inhibitory and excitatory inputs from distinct upstream brain areas to regulate the selection of appropriate active or passive defensive behaviours.

Discussion

Our study defines an amygdala–midbrain–medullary circuit through which freezing behaviour, an evolutionarily conserved response to threat, is generated. Central to this process is a circuit mechanism involving the disinhibition of vlPAG glutamatergic neurons projecting to pre-motor cells located in the Mc. Disinhibition of this vlPAG→Mc pathway is generated by a disynaptic GABAergic local micro-circuit receiving inhibitory input from CEA (Extended Data Fig. 6). It is important to note that the excitatory vlPAG to Mc pathway did not mediate concomitant analgesia, a hallmark of the general defensive response to threat. Consistent with this result, our single-unit data show that some glutamatergic neurons of the vlPAG are positively and others are negatively correlated with freezing behaviour. These findings suggest that different aspects of the defensive response, such as freezing, flight and analgesia, could be mediated by distinct glutamatergic output pathways from the PAG.

Our data suggest the existence of a dedicated vlPAG output mediating freezing. However, to ensure a rapid switch between passive and active coping with fluctuating threat levels, interactions between freezing and flight circuits are required. Active defensive behaviour including flight could be driven by different hypothalamic[26,27] or prefrontal[43] inputs, directly or via disinhibition onto dl/lPAG glutamatergic neurons, which concomitantly might block freezing behaviour by activation of GABAergic neurons controlling excitatory vlPAG output to the medulla. This notion is supported by our finding of glutamatergic inputs from dl/lPAG onto GABAergic neurons of the vlPAG. While earlier models of PAG function have emphasized its columnar organization[13,17,19,34,44,45], or the existence of parallel input-output pathways mediating active or passive defensive behaviours[3,12,46], the model emerging from our study supports a key role for local PAG circuitry in the integration of extrinsic inputs to ensure rapid behavioural, autonomic and endocrine adaptations in the face of threat.

A growing body of evidence suggests that the interactions of distinct types of neuron within highly organized neuronal circuits are critical for any higher brain function[47–49], and that circuit dysregulation contributes to psychiatric conditions, among which fear

and anxiety-related disorders are the most prevalent[4,5,50]. Our study shows that similar organizational principles and functional motifs exist even within evolutionarily old, mammalian 'survival circuits'[3] dedicated to expression of defensive behaviours. A mechanistic functional understanding of these circuits will provide new insights into possible mechanisms underlying human psychiatric conditions associated with maladaptive coping behaviours under stressful conditions.

Online Content Methods, along with any additional Extended Data display items and Source Data, are available in the online version of the paper; references unique to these sections appear only in the online paper.

Received 10 September 2015; accepted 8 April 2016.
Published online 1 June 2016.

1. Anderson, D. J. & Adolphs, R. A framework for studying emotions across species. *Cell* **157,** 187–200 (2014).
2. Blanchard, D. C. & Blanchard, R. J. in *Handbook of Anxiety and Fear* Vol. 17 (eds Blanchard, R. J., Blanchard, D. C., Griebel, G. & Nutt, D.) Ch. 2.4, 63–79 (Academic, 2008).
3. LeDoux, J. Rethinking the emotional brain. *Neuron* **73,** 653–676 (2012).
4. Deisseroth, K. Circuit dynamics of adaptive and maladaptive behaviour. *Nature* **505,** 309–317 (2014).
5. Tovote, P., Fadok, J. P. & Lüthi, A. Neuronal circuits for fear and anxiety. *Nature Rev. Neurosci.* **16,** 317–331 (2015).
6. Rosen, J. B. & Schulkin, J. From normal fear to pathological anxiety. *Psychol. Rev.* **105,** 325–350 (1998).
7. Perusini, J. N. & Fanselow, M. S. Neurobehavioral perspectives on the distinction between fear and anxiety. *Learn. Mem.* **22,** 417–425 (2015).
8. Blanchard, D. C., Griebel, G., Pobbe, R. & Blanchard, R. J. Risk assessment as an evolved threat detection and analysis process. *Neurosci. Biobehav. Rev.* **35,** 991–998 (2011).
9. Blanchard, R. J. & Blanchard, D. C. Crouching as an index of fear. *J. Comp. Physiol. Psychol.* **67,** 370–375 (1969).
10. Fanselow, M. S. & Bolles, R. C. Naloxone and shock-elicited freezing in the rat. *J. Comp. Physiol. Psychol.* **93,** 736–744 (1979).
11. Blanchard, D. C., Griebel, G. & Blanchard, R. J. Mouse defensive behaviors: pharmacological and behavioral assays for anxiety and panic. *Neurosci. Biobehav. Rev.* **25,** 205–218 (2001).
12. Gross, C. T. & Canteras, N. S. The many paths to fear. *Nature Rev. Neurosci.* **13,** 651–658 (2012).
13. Carrive, P. The periaqueductal gray and defensive behavior: functional representation and neuronal organization. *Behav. Brain Res.* **58,** 27–47 (1993).
14. Leman, S., Dielenberg, R. A. & Carrive, P. Effect of dorsal periaqueductal gray lesion on cardiovascular and behavioural responses to contextual conditioned fear in rats. *Behav. Brain Res.* **143,** 169–176 (2003).
15. Tomaz, C., Brandão, M., Bagri, A., Carrive, P. & Schmitt, P. Flight behavior induced by microinjection of GABA antagonists into periventricular structures in detelencephalated rats. *Pharmacol. Biochem. Behav.* **30,** 337–342 (1988).
16. Walker, P. & Carrive, P. Role of ventrolateral periaqueductal gray neurons in the behavioral and cardiovascular responses to contextual conditioned fear and poststress recovery. *Neuroscience* **116,** 897–912 (2003).
17. Zhang, S. P., Bandler, R. & Carrive, P. Flight and immobility evoked by excitatory amino acid microinjection within distinct parts of the subtentorial midbrain periaqueductal gray of the cat. *Brain Res.* **520,** 73–82 (1990).
18. Morgan, M. M. & Clayton, C. C. Defensive behaviors evoked from the ventrolateral periaqueductal gray of the rat: comparison of opioid and GABA disinhibition. *Behav. Brain Res.* **164,** 61–66 (2005).
19. Fanselow, M. S. in *The Midbrain Periaqueductal Gray Matter: Functional, Anatomical and Immunohistochemical Organization* (eds Depaulis, A. & Bandler, R.) 151–173 (Plenum, 1991).
20. Bandler, R., Depaulis, A. & Vergnes, M. Identification of midbrain neurones mediating defensive behaviour in the rat by microinjections of excitatory amino acids. *Behav. Brain Res.* **15,** 107–119 (1985).
21. Bandler, R. & Carrive, P. Integrated defence reaction elicited by excitatory amino acid microinjection in the midbrain periaqueductal grey region of the unrestrained cat. *Brain Res.* **439,** 95–106 (1988).
22. Tovote, P. *et al.* Activation of central CRF receptor 1 by cortagine results in enhanced passive coping with a naturalistic threat in mice. *Psychoneuroendocrinology* **35,** 887–895 (2010).
23. Rizvi, T. A., Ennis, M., Behbehani, M. M. & Shipley, M. T. Connections between the central nucleus of the amygdala and the midbrain periaqueductal gray: topography and reciprocity. *J. Comp. Neurol.* **303,** 121–131 (1991).
24. Oka, T., Tsumori, T., Yokota, S. & Yasui, Y. Neuroanatomical and neurochemical organization of projections from the central amygdaloid nucleus to the nucleus retroambiguus via the periaqueductal gray in the rat. *Neurosci. Res.* **62,** 286–298 (2008).
25. Canteras, N. S., Simerly, R. B. & Swanson, L. W. Projections of the ventral premammillary nucleus. *J. Comp. Neurol.* **324,** 195–212 (1992).
26. Silva, B. A. *et al.* Independent hypothalamic circuits for social and predator fear. *Nature Neurosci.* **16,** 1731–1733 (2013).
27. Wang, L., Chen, I. Z. & Lin, D. Collateral pathways from the ventromedial hypothalamus mediate defensive behaviors. *Neuron* **85,** 1344–1358 (2015).
28. An, X., Bandler, R., Ongür, D. & Price, J. L. Prefrontal cortical projections to longitudinal columns in the midbrain periaqueductal gray in macaque monkeys. *J. Comp. Neurol.* **401,** 455–479 (1998).
29. Choi, J. S. & Kim, J. J. Amygdala regulates risk of predation in rats foraging in a dynamic fear environment. *Proc. Natl Acad. Sci. USA* **107,** 21773–21777 (2010).
30. Behbehani, M. M. Functional characteristics of the midbrain periaqueductal gray. *Prog. Neurobiol.* **46,** 575–605 (1995).
31. Depaulis, A., Morgan, M. M. & Liebeskind, J. C. GABAergic modulation of the analgesic effects of morphine microinjected in the ventral periaqueductal gray matter of the rat. *Brain Res.* **436,** 223–228 (1987).
32. Vaughan, C. W., Ingram, S. L., Connor, M. A. & Christie, M. J. How opioids inhibit GABA-mediated neurotransmission. *Nature* **390,** 611–614 (1997).
33. Ciocchi, S. *et al.* Encoding of conditioned fear in central amygdala inhibitory circuits. *Nature* **468,** 277–282 (2010).
34. LeDoux, J. E. Emotion circuits in the brain. *Annu. Rev. Neurosci.* **23,** 155–184 (2000).
35. Knobloch, H. S. *et al.* Evoked axonal oxytocin release in the central amygdala attenuates fear response. *Neuron* **73,** 553–566 (2012).
36. Wall, N. R., Wickersham, I. R., Cetin, A., De La Parra, M. & Callaway, E. M. Monosynaptic circuit tracing *in vivo* through Cre-dependent targeting and complementation of modified rabies virus. *Proc. Natl Acad. Sci. USA* **107,** 21848–21853 (2010).
37. Fenno, L. E. *et al.* Targeting cells with single vectors using multiple-feature Boolean logic. *Nature Methods* **11,** 763–772 (2014).
38. Herry, C. *et al.* Switching on and off fear by distinct neuronal circuits. *Nature* **454,** 600–606 (2008).
39. Lima, S. Q., Hromádka, T., Znamenskiy, P. & Zador, A. M. PINP: a new method of tagging neuronal populations for identification during *in vivo* electrophysiological recording. *PLoS ONE* **4,** e6099 (2009).
40. Esposito, M. S., Capelli, P. & Arber, S. Brainstem nucleus MdV mediates skilled forelimb motor tasks. *Nature* **508,** 351–356 (2014).
41. Orlovsky, G. N., Deliagina, T. G. & Grillner, S. in *Neuronal Control of Locomotion: From Mollusc to Man* Ch. 10 and 12 (Oxford Univ. Press, 1999).
42. Stamatakis, A. M. *et al.* A unique population of ventral tegmental area neurons inhibits the lateral habenula to promote reward. *Neuron* **80,** 1039–1053 (2013).
43. Halladay, L. R. & Blair, H. T. Distinct ensembles of medial prefrontal cortex neurons are activated by threatening stimuli that elicit excitation vs. inhibition of movement. *J. Neurophysiol.* **114,** 793–807 (2015).
44. Keay, K. A. & Bandler, R. Parallel circuits mediating distinct emotional coping reactions to different types of stress. *Neurosci. Biobehav. Rev.* **25,** 669–678 (2001).
45. Depaulis, A., Keay, K. A. & Bandler, R. Longitudinal neuronal organization of defensive reactions in the midbrain periaqueductal gray region of the rat. *Exp. Brain Res.* **90,** 307–318 (1992).
46. Vianna, D. M., Landeira-Fernandez, J. & Brandão, M. L. Dorsolateral and ventral regions of the periaqueductal gray matter are involved in distinct types of fear. *Neurosci. Biobehav. Rev.* **25,** 711–719 (2001).
47. Letzkus, J. J. *et al.* A disinhibitory microcircuit for associative fear learning in the auditory cortex. *Nature* **480,** 331–335 (2011).
48. Wolff, S. B. *et al.* Amygdala interneuron subtypes control fear learning through disinhibition. *Nature* **509,** 453–458 (2014).
49. Hangya, B., Pi, H. J., Kvitsiani, D., Ranade, S. P. & Kepecs, A. From circuit motifs to computations: mapping the behavioral repertoire of cortical interneurons. *Curr. Opin. Neurobiol.* **26,** 117–124 (2014).
50. Lüthi, A. & Lüscher, C. Pathological circuit function underlying addiction and anxiety disorders. *Nature Neurosci.* **17,** 1635–1643 (2014).

Supplementary Information is available in the online version of the paper.

Acknowledgements We thank C. Müller, J. Lüdke, K. Bylund, J. Alonso, T. Lu, P. Argast and P. Buchmann for technical assistance, J. J. Letzkus for input on the manuscript, and all members of the Lüthi and Arber laboratories for discussions and other help with the project. We thank L. Gelman and S. Bourke for help with microscopy, and M. Stadler for statistical advice. We are grateful to G. Keller for providing viruses for optogenetics, Z. J. Huang for initially providing the *Gad2-ires-Cre* mouse line and L. Xiao and P. Scheiffele for the anti-rabiesG antibody. This work was supported by the Novartis Research Foundation, by the National Center of Competences in Research: 'SYNAPSY — The Synaptic Bases of Mental Diseases' (financed by the Swiss National Science Foundation) as well as by a Swiss National Science Foundation Core Grant, and a European Research Council Advanced Grant to A.L. Support for S.A. and M.S.E. was provided by a European Research Council Advanced Grant, the Swiss National Science Foundation and the Kanton Basel-Stadt. P.T. and J.P.F. were supported by NARSAD Young Investigator Grants by the Brain and Behavior Foundation. M.S.E. was also supported by a long-term post-doctoral fellowship of the Human Frontier Science Program and a Synapsis Foundation Grant. F.C. and C.H. were supported by grants from the European Research Council (ERC)

under the European Union's Seventh Framework Program (FP7/2007-2013)/ERC grant agreement number 281168 and the Fondation pour la Recherche Médicale.

Author Contributions P.T. conceived, designed, performed and analysed most of the experiments and wrote the manuscript. M.S.E. conceived, designed, performed and analysed neuroanatomical tracing experiments. P.B. performed and analysed *in vitro* slice recordings. F.C. and C.H. performed single-unit recordings in the PAG. S.B.E.W. established optogenetic methodology. J.P.F. performed experiments. M.M. designed and tested viruses for optogenetics. C.R., L.F. and K.D. produced viruses for optogenetics. S.A. designed viruses for tracing and optogenetics. A.L. conceived the project and wrote the manuscript. All authors contributed to the experimental design and commented on the manuscript.

Author Information Reprints and permissions information is available at www.nature.com/reprints. The authors declare no competing financial interests. Readers are welcome to comment on the online version of the paper. Correspondence and requests for materials should be addressed to P.T. (philip.tovote@fmi.ch) or A.L. (andreas.luthi@fmi.ch).

METHODS

Animals. Experimental subjects were adult (2- to 5-month-old) male, wild-type (Charles River Laboratories) or mutant mice of the C57BL/6J strain. *Slc17a6*$^{tm2(cre)Lowl}$ (*Vglut2-ires-Cre*) and *Chat*$^{tm2(cre)Lowl}$ (*Chat-ires-Cre*) mice were obtained from Jackson Laboratories. Founders for a *Gad2*$^{tm2(cre)Zjh}$ (*Gad2-ires-Cre*) and *Gad1–eGFP* mice colony were initially provided by Z. J. Huang. *Tau-lox-stop-lox–SynGFP–IRES-nlsLacZpA* mice came from an in-house colony[40]. All mice were individually housed in a 12 h light/dark cycle and all experiments were performed during the light cycle. Food and water was available *ad libitum*. Sample sizes were estimated based on previous studies using similar experimental designs[26,33,38,40,47]. All animal procedures were performed in accordance with institutional guidelines and were approved by the Veterinary Department of the Canton of Basel-Stadt.

Viral injections and optogenetics. Isoflurane (Attane, induction 3%, maintenance 1.5%; Provet) in oxygen-enriched air (Oxymat 3; Weinmann) was used to anaesthetize mice fixed in a stereotactic frame (Kopf Instruments 1900 series). Before opening of the scalp, local injections of ropivacain (Naropin; AstraZeneca) provided analgesia during surgery. After completion of surgery, intraperitoneal injections of meloxicam were administered to alleviate pain (60 μl of 0.5 mg ml^{-1}, Metacam; Boehringer). A feedback-controlled heating pad (FHC) ensured maintenance of core body temperature at 36 °C. A volume of 50–200 nl virus solution (depending on respective viral titre and observed expression strength) was pressure-injected intracranially using calibrated glass pipets (5 μl microcapillary tube; Sigma-Aldrich) connected to a picospritzer III (Parker). To avoid the subcranial midline blood sinus targeting the vlPAG, holes with a diameter of 0.3 mm were drilled bilaterally into the skull at ±1.7 mm (dl/lPAG: ±1.4 mm) from midline suture, and at the level of the lambda suture. The injection capillary was then slowly lowered using a hydraulic micropositioner (Kopf Instruments model 2650) at a zenith angle of 26° to the target depth of 3 mm (dl/lPAG: ±2.6 mm) below brain surface. Coordinates for CEA injections were −1.1 mm caudal and ±2.7 mm mediolateral to bregma, at −4.2 mm perpendicularly below brain surface. The Mc of the medulla was targeted with bilateral perpendicular injections −6.4 mm caudal and ±0.95 mm mediolateral to bregma, with an injection depth of 5.6 mm. Cell-type-specific expression of optical actuators was achieved using the following, Cre-dependent AAV: rAAV(2/5)/EF1a-flex-hChR2(T159C)–mCherry (UNC Vector Core), rAAV(2/9)/CAG-flex-ReaChR-Citrine–YFP–WPRE (custom design, Vector Biolabs), rAAV(2/7) EF1a-flex-ChR2(H134R)-2A-NpHR-2A-Venus[47] and rAAV(2/5)CBA-flex-ARCH–GFP[48]. For characterization of the functional connection between GABAergic and glutamatergic neurons in the vlPAG, we introduced ChR2 into vGluT2^{-}, putative GABAergic neurons in the vlPAG using a double-conditional approach in *Vglut2-ires-Cre mice*. We co-injected two AAVs: one that delivered Flp recombinase in an unconditional manner and one that mediated expression of ChR2 only in the presence of Flp and in the absence of Cre (AAVdj/hSyn- Cre^{OFF}-Flp^{ON}-hChR2(H134R)–eYFP)[37]. Visual targeting of vGluT2^{+} neurons was achieved by Cre-dependent expression of tdTomato (rAAV(2/9)-flex-tdTomato). For Cre- and Flp- dependent expression of ChR2 in the glutamatergic vlPAG-to-Mc projection, we combined an injection of a retrogradely trafficked HSV (HSV/hEF1a-LS1L–mCherry–IRES-flpo; R. Neve) into the Mc with another injection of AAV(dj)/hSyn-Cre^{ON}/Flp^{ON}-hChR2(H134R)–mCherry[37] into the vlPAG of *Vglut2-ires-Cre* mice. Control mice were injected with the following AAVs: AAV(2/5)EF1a-flex-tdTomato (provided by G. Keller), AAV(2/9)CAG-flex–eGFP–WPRE-bGH, AAV(2/9)CAG-flex-tdTomato-WPRE-bGH (both Penn Vector) and AAV(dj)/hSyn-Cre^{ON}/Flp^{ON}–mCherry[37].

For optical manipulation or electrophysiological recordings, mice were implanted with custom-built fibre connectors (fibre: 0.48 numerical aperture, 200 μm diameter; Thorlabs) 3–4 weeks after virus injections. The tip of the fibre was lowered at an angle of 26° to 250 μm above the injection site in the PAG. Implants were fixed to the skull with skull screws (P.A. Precision Components), cyanoacrylate glue (Ultra Gel; Henkel) and dental cement (Paladur; Heraeus). All fibre connectors were tested for effective light transduction before implantation. For optical stimulation of ChR2, laser light of 473 nm (CNI Laser) was applied, whereas laser light of 594 nm was used for optical stimulation of NpHR or Arch. Light intensity was adjusted with an optical power meter (Thorlabs) to reach 10–15 mW at the end of the implanted fibre stub.

Histology. After completion of experiments, mice were transcardially perfused with 4% paraformaldehyde in phosphate-buffered saline (PBS). Fixed brains were cryoprotected in 30% sucrose/PBS and cut on a cryostat in 80 μm coronal slices. Antibody stainings were performed on single-well floating tissue sections. Sections were incubated for 48 h in primary antibodies at 4 °C followed by one overnight incubation with secondary antibodies at 4 °C. Primary antibodies used in this study were as follows: chicken anti-GFP 1:1,000 (A10262, Molecular Probes), rabbit anti-RFP 1:5,000 (600-401-379, Rockland Immunochemicals), guinea pig anti-vGlut2 1:5,000 (AB5907, Chemicon), mouse anti-V5 1:1,000 (R960CUS, Invitrogen), mouse anti-NeuN 1:1,000 (MAB377, Chemicon), mouse anti-Myc 1:100 (CRL-1729, ATCC), goat anti-Bgal 1:4,000 (AR2282, Biogenesis), mouse anti-channelrhodopsin-2 1:2 (clone 15E2, 651180, PROGEN Biotechnik), guinea pig anti-rabiesG 1:500 (provided by P. Scheiffele). Fluorophore-tagged secondary antibodies used were Alexa Fluor 488 donkey anti-chicken IgY 1:1,000 (703-545-155, Jackson), Cy3 donkey anti-rabbit IgG 1:1,000 (711-165-152, Jackson), Alexa Fluor 657 donkey anti-guinea pig IgG 1:1,000 (706-605-148, Jackson), Alexa Fluor 657 donkey anti-mouse IgG 1:1,000 (715-605-150, Jackson), Alexa Fluor 657 donkey anti-goat IgG 1:1,000 (705-605-147, Jackson) or Alexa Fluor 488 donkey anti-mouse IgG 1:1,000 (A21202, Molecular Probes). For counterstaining, sections were incubated for 10 min with 4′,6-diamidin-2-phenylindol (DAPI, 1:10,000, Sigma). Stained brain sections were mounted on gelatin-coated slides and coverslipped with custom-made glycerol-based medium (Fluorostab). Slides were imaged using an automated slide scanner microscope (Zeiss Axioscan).

Placement of the optical fibres was assessed on the basis of the lesion the fibre tip inside the brain tissue. Mice with no or unilateral expression of the virus, or fibre tip placement outside of the PAG, were excluded from the analysis. To analyse virus expression in *Vglut2-ires-Cre* mice expressing ChR2(T159C), we outlined the area of somatic viral expression on the respective sections in a mouse brain atlas[51] for each animal, and then overlaid the areas at 30% transparency (Adobe Illustrator) to visualize the average centre of expression in each behavioural group.

Behaviour. Mice of different litters but the same genotype were used in individual experiments. No criteria were used to allocate mice to experimental groups, and, for blinding, experimental subjects had unique letter/number identifiers that indicated genotype but no group assignment. All basic testing of light-induced behavioural effects was performed under low-fear conditions in a novel, circular Plexiglas cylinder with smooth white floor (diameter 27 cm) under dim-light conditions in a dark-walled sound-attenuated chamber. Acetic acid (1%) was used to clean the context and to provide a distinct olfactory stimulus. After 1 min of habituation, light was applied four times for 5 s, with an inter-stimulus interval of 55 s. Total duration of freezing during the four 'light on' periods was compared with time spent freezing in the period of equivalent length immediately before onset of the first light stimulus.

To investigate light-mediated effects on conditioned freezing, mice were subjected to auditory fear conditioning in a brightly illuminated square context (27 cm × 27 cm) with a metal grid floor. A train of 20 tone beeps (7.5 kHz, 75 dB sound pressure level, 500 ms duration, 500 ms inter-beep-interval) was used as the conditioned stimulus (CS) and an electrical foot-shock (0.6 mA dc, 1 s duration) was used as the unconditioned stimulus (US). The conditioning session lasted 440 s during which the mice were exposed to three back-to-back CS–US pairings in a pseudo-random fashion, with a baseline period of 180 s and a minimal inter-stimulus interval of 80 s. On the day after conditioning, mice were exposed to four CS-only presentations in a dimly illuminated context different from the conditioning context. While the conditioning context was cleaned with 70% ethanol, the retrieval context was wiped down with 1% acetic acid. The duration of the retrieval session was 540 s, with a baseline period of 180 s and a pseudo-random presentation of the CS with a minimal inter-stimulus interval of 120 s. To test for light-activation effects on CS-induced defensive behaviour, the second and fourth presentation of the CS was paired with 20 s of continuous laser light. Total duration of freezing during the two CS-alone periods (first and third) was compared with time spent freezing during the two CS periods (second and fourth) paired with 'light on', and with a baseline period of equal length (40 s) directly before onset of the first CS. Contextual fear was tested a day later by re-introducing the experimental subject into the original conditioning context for 5 min. To test for effects of light activation on contextual freezing laser illumination was turned on twice for 1 min, with a 1 min pre-baseline and a 1 min inter-stimulus interval. Total duration of freezing during the two 'light on' periods was compared with time spent freezing in the time period of equivalent length immediately before light onset.

For *in vivo* recordings of unidentified PAG single units, auditory fear conditioning and testing took place in two different contexts (contexts A and B). To measure movement, an automated infrared beam detection system located on the bottom of the experimental chambers was used (Coulbourn Instruments). The animals were considered to be freezing if no movement was detected for 2 s (ref. 38). On day 1, C57BL6/J mice were submitted to a habituation session in context A, in which they received four presentations of the CS^{+} and the CS^{-} (total CS duration, 30 s; consisting of 50-ms pips at 0.9 Hz repeated 27 times, 2 ms rise and fall, pip frequency, 7.5 kHz or white-noise, 80 dB sound pressure level). Discriminative fear conditioning was performed on the same day by pairing the CS^{+} with a US (1 s foot-shock, 0.6 mA, 5 CS^{+}–US pairings, inter-trial intervals, 20–180 s). The onset of the US coincided with the offset of the CS^{+}. The CS^{-} was presented after each CS^{+}–US association but was never reinforced (five CS^{-} presentations; inter-trial intervals, 20–180 s). The frequencies used for CS^{+} and CS^{-} were counterbalanced

across animals. On day 2, conditioned mice were submitted to a testing session (retrieval session) in context B during which they received four presentations of the CS^- and CS^+.

To test for effects on unconditioned freezing, mice were exposed to a remote-controlled toy snake in an open-field arena (50 cm × 50 cm). To control for baseline activity and laser effects, mice were pre-exposed to the open field alone for 10 min, with four laser illumination periods of 20 s (inter-stimulus interval 40 s) in the second half of this phase. After introduction of the snake, mice remained in the open field for another 5 min, during which the snake's movement was remotely controlled by the experimenter outside the chamber. To maintain high freezing levels, the snake was moved around the area, thereby covering varying distances to the mouse without establishing direct contact.

Locomotor activity was recorded by an infrared beam system (Coulbourn Instruments) or an overhead video tracking system (CinePlex Studio). Freezing was defined as immobility detected by lack of beam breaks for 2 s, as described before[38]. Using the video tracking system, freezing was extracted with the freezing detector plug-in (CinePlex Editor). A 2 s criterion of the thresholded motion measure, based on a contour-tracking algorithm, was used to define freezing. Motion measure was automatically computed as the normalized frame-by-frame difference of the animal's body contour in pixels. Automatically detected freezing behaviour was cross-checked on the video recording to exclude false-positive freezing bouts, for example during grooming episodes, or include false negative freezing intervals, for example owing to motion artefacts caused by cable movement in front of the camera. Timestamps for freezing episodes and stimulation events (CS, US, laser) were imported into data analysis software (Neuroexplorer 5, Nex Technologies) and averaged over the respective time interval. Behavioural activity of the animal was assessed using the motion measure of the video tracking system. Motion was averaged over 1-s bins and normalized as the percentage change in relation to a baseline period. Baseline was the time directly before stimulus onset: that is, 16 s before 'light on' in experiments with naive mice, and 10 s before CS/CS^+'light on' in cued fear-conditioning experiments. Combined contour tracking of the mouse and colour-tracking of the toy snake were used to extract *x*–*y* coordinates of the two subjects and calculate their distance.

Tail immersion test. To test for analgesic effects induced by optical stimulation of glutamatergic cells of the PAG, mice tail tips were immersed in hot water with a temperature of 50 °C. This was done eight times with an inter-trial interval of 40 s, and tail withdrawal latency was scored frame-by-frame (Windows Live Movie Maker) from the video recorded during the test session (Plexon Cineplex). On the last four trials, laser light was turned on for 5 s directly before the tail immersion. If the mouse did not withdraw its tail within 10 s of immersion, the trial was terminated. Tail withdrawal latencies of the first four non-manipulated trials were averaged as baseline and compared with average withdrawal latency during the last four light-stimulated trials.

Slice electrophysiology. Standard procedures were used to prepare 300 μm thick coronal slices from 12- to 14-week-old male *Vglut2-ires-Cre* or *Vglut2-ires-Cre::Gad1–eGFP* mice, which received intracranial virus injections 4 weeks before. The brain was dissected in ice-cold artificial cerebrospinal fluid, mounted on an agar block and sliced with a vibrating-blade microtome (HM 650 V, Carl Zeiss) at 4 °C. Slices were maintained for 45 min at 37 °C in an interface chamber containing artificial cerebrospinal fluid equilibrated with 95% O_2/5% CO_2 and containing the following (in mM): 124 NaCl, 2.7 KCl, 2 $CaCl_2$, 1.3 $MgCl_2$, 26 $NaHCO_3$, 0.4 NaH_2PO_4, 18 glucose, 4 ascorbate. Recordings were performed with artificial cerebrospinal fluid in a recording chamber at a temperature of 35 °C at a perfusion rate of 1–2 ml min^{-1}. PAG neurons were visually identified with infrared video microscopy using an upright microscope equipped with a ×40 objective (Olympus). Patch electrodes (3–5 MΩ) were pulled from borosilicate glass tubing. For voltage clamp experiments to record eIPSCs, patch electrodes were filled with a solution containing the following (in mM): 110 CsCl, 30 K-gluconate, 1.1 EGTA, 10 HEPES, 0.1 $CaCl_2$, 4 Mg-ATP, 0.3 Na-GTP (pH adjusted to 7.3 with CsOH, 280 mOsm) and 4 *N*-(2,6-dimethylphenylcarbamoylmethyl) triethylammonium bromide (QX-314; Tocris-Cookson).

Evoked IPSCs were elicited by 10 ms blue-light stimulation of either local vlPAG axon terminals of non-glutamatergic neurons expressing ChR2 or $ChR2^+$ CEA axons projecting to PAG. To exclude glutamatergic inputs, CNQX (6-cyano-7-nitroquinoxaline-2,3-dione, 10 μM: AMPA receptor antagonist) and (R)-CPP ((RS)-3-(2-carboxypiperazin-4-yl)-propyl-1-phosphonic acid, 10 μM: NMDA receptor antagonist) were added to the artificial cerebrospinal fluid. To confirm the eIPSCs GABAergic nature, picrotoxin (100 μM) was added at the end of the recordings. Successful connections were scored if the amplitude of eIPSCs was higher than 10 pA, with the latency within 10 ms for at least 60% of the trials (six out of ten trials). Whole-cell patch-clamp recordings were excluded if the access resistance exceeded 13 MΩ and changed more than 20% during the recordings. Data were recorded with a MultiClamp 700B (Molecular Devices) amplifier, filtered at 0.2 kHz and digitized at 10 kHz. Data were acquired and analysed with Clampex 10.0, Clampfit 10.0 (Molecular Devices). All chemicals for the internal and external solutions were purchased from Fluka/Sigma. Glutamatergic blockers were purchased from Tocris Bioscience.

Anatomical tracing. To characterize CEA inputs to vlPAG, we injected retrogradely transported fluorescent latex beads (Lumafluor) into the vlPAG of two *Gad1–eGFP* mice. Four days after injection, mice were killed, transcardially perfused with 4% paraformaldehyde in PBS, and brains were extracted and processed for histology as described above. On four coronal sections from each mouse, $bead^+$ cells in the CEl and CEm were counted and normalized against total cells stained by NeuN.

To identify the presynaptic partners of specific neuronal subpopulations in the PAG, we used a monosynaptically restricted pseudotyped rabies virus[36]. We performed a local injection in the vlPAG or lPAG of AAVs conditionally delivering rabies glycoprotein (AAV(2/9)CAG-flex-rabiesG-2A-H2B-10xV5-tag, short: AAV-flex-rabiesG)[40] and TVA (AAV(2/9)CAG-flex-TVA-2A-H2B–eGFP, short: AAV-flex-TVA)[40] into either *Vglut2-ires-Cre* or *Gad2-ires-Cre* mice. Two weeks later, we injected EnvA-ΔG–mCherry–rabies[36] into the same location. Mice were killed 7 days thereafter, transcardially perfused with 4% paraformaldehyde in PBS, and brains were extracted and processed for histology as described above. Brain sections corresponding to the injection site were stained for GFP, red fluorescent protein (RFP) and V5, and counterstained with DAPI. Brain sections outside the injection site were stained for RFP and NeuN. To compare the relative input to the different PAG subpopulations, we quantified the number of starter cells within the PAG (mCherry, GFP and V5 triple-positive cells) in four sections around the injection site and we counted the number of $mCherry^+$ cells within the entire CEA. Images were acquired with an Olympus confocal microscope (FV1000) with a motorized stage, using a ×20 objective, a 3 × 3 tiled scan with 15% overlap and a step size of 1.5 μm along the depth of the slice. Triple-positive cells in the PAG and $mCherry^+$ cells in CEA were counted manually along every confocal plane using Imaris software (Bitplane). To quantify the hypothalamic input to PAG subpopulations, we analysed approximately half the volume of the hypothalamus by imaging every other section along the rostro-caudal axis with an automated slide scanning microscope (Zeiss Axioscan Z1) using a ×10 objective. $mCherry^+$ neurons were counted manually on the image projection. We use the following nomenclature for the hypothalamic nuclei: dorsomedial hypothalamic nucleus (DM), anterior hypothalamus, medial part (AHM, including the entire anterior hypothalamic area, the latero-anterior hypothalamic nucleus and the paraventricular hypothalamic nucleus), ventromedial hypothalamic nucleus (VMH), posterior hypothalamic nucleus (PH), peduncular part of lateral hypothalamus (PLH, including the Mc of the lateral hypothalamus), lateral hypothalamic area (LH, including the parasubthalamic nucleus), premammillary nucleus (PMD). All quantifications were performed by an experimenter blind to the subject's genotype.

To study PAG projections to brainstem neurons directly connected to spinal motor neurons (pre-motor neurons), we combined an anterograde vlPAG injection of an AAV expressing presynaptic fluorescent markers and monosynaptic rabies spreading from spinal motor neurons. To label pre-motor neurons, we injected a monosynaptic rabies virus into forelimb muscles that retrogradely infected the corresponding spinal motor neurons. To allow for spreading of the rabies virus in adult mice, we complemented cervical motor neurons with an AAV conditionally expressing rabies glycoprotein through an intra-spinal injection in *ChAT-Cre* mice. First, we injected into the vlPAG of *ChAT-Cre* adult mice a custom-made AAV that unconditionally expressed GFP-tagged synaptophysin (Syn) in presynaptic terminals (AAV(2/9)/CAG-flex-SynGFP + AAV(2/9)/CMV-Cre)[40]. In the same surgery session, we injected AAV(2/9)CAG-flex-rabiesG-2A-H2B-10xV5-tag[40] into the cervical part of the spinal cord. Two weeks thereafter, G-deleted rabies virus coated with the CVS-glycoprotein was injected in triceps and biceps muscles. Eight days after rabies injection, mice were killed and brains were immunostained against GFP, RFP and vGluT2 and counterstained with DAPI. High-resolution three-dimensional images of eight complete pre-motor cells in the Mc were acquired on a custom-made dual motorized spinning-disk microscope (Life Imaging Services) using a ×63 objective, 8 × 8 tile scan and 0.2 μm step size. We quantified the number of GFP^+ ($vGluT2^+$) vlPAG inputs to soma and dendritic tree of these cells manually in eight neurons from three mice. The Mc was defined as described before[40] and included lateral paragigantocellular, as well as ventral and alpha parts of the gigantocellular, reticular nucleus.

To assess local vlPAG inputs specifically onto Mc-projecting glutamatergic neurons, we used an intersectional viral approach (Extended Data Fig. 4f–h). We injected a retrogradely transported HSV that Cre-dependently delivered rabies G-protein (HSV/hEF1α-LS1L-rabiesG; R. Neve) into the Mc of offspring from *Vglut2-ires-Cre* crossed with *Gad1–eGFP* mice. In the same surgery session, we

injected conditional AAV into the vlPAG to virally express the TVA receptor in glutamatergic cells (rAAV(2/9)CAG-flex-TVA-2A-H2B–eGFP, custom designed, Vector Biolabs). Two weeks later, we injected EnvA-ΔG–mCherry–rabies into the Mc. Mice were killed 7 days later and brains processed as described above. We then used standard immunohistochemistry to stain for GFP, RFP and rabies G-protein. High-resolution confocal images (×40) of vlPAG were taken from three coronal sections of the PAG (rostral, medial, caudal) and individual cells were manually counted using Imaris software (Bitplane). Triple-positive cells were identified as starter cells, whereas GFP and RFP double-positive cells represented local GAD1$^+$ cells connected to glutamatergic Mc-projecting neurons.

We performed several controls to demonstrate the specificity of the monosynaptic rabies tracing technology. To check for the specificity of the AAV viruses delivering the TVA receptor (AAV-flex-TVA) and rabiesG protein (AAV-flex-rabiesG), we injected those viruses in the vlPAG of offspring from *Vglut2-Cre* and *Tau-lox-stop-lox-SynGFP–IRES-nlsLacZpA* reporter mouse lines. After 2 weeks, animals were killed and the injection site was cut, immunostained and co-localization of GFP or V5 with b-Gal was analysed. In an additional experiment, *Vglut2-ires-Cre* animals were injected with AAV-flex-TVA followed by EnvA-ΔG–mCherry–rabies 2 weeks later. Furthermore, to test for the leakiness of the EnvA-ΔG–mCherry–rabies, we injected this virus in the vlPAG of wild-type animals combined with latex beads. Animals were killed 1 week later and the entire PAG, amygdala and hypothalamus were cut and stained for mCherry and NeuN. Lastly, wild-type animals were injected with AAV-flex-TVA, AAV-flex-rabiesG and EnvA-ΔG–mCherry–rabies following the same protocol used for monosynaptic tracing experiments.

To characterize the connectivity from dlPAG to vlPAG, we injected AAV(2/9) CAG-flex-Synaptophysin-Myc[40] into offspring of *Vglut2-ires-Cre* mice crossed with *Gad1–eGFP* mice ($n = 4$ mice) to visualize glutamatergic dlPAG contacts onto GFP$^+$ GABAergic vlPAG neurons. To quantify opposing synaptic contacts, we selected neurons with complete soma and acquired ×60 confocal images at a step size of 0.2 μm with a confocal microscope (Olympus FV1000). Quantification of synaptic inputs from ipsilateral ($n = 21$ cells from four mice) and contralateral ($n = 13$ cells from two mice) hemispheres was performed manually using Imaris software (Bitplane).

Single-unit recordings. Custom-built, chronically implanted 16-wire electrodes[38] were used to record electrical activity in the vlPAG. Electrodes were connected to a headstage (Plexon) containing 16 unity-gain operational amplifiers. The headstage was connected to a 16-channel preamplifier (gain 100 × bandpass filter from 150 Hz to 9 kHz for unit activity, Plexon). Spiking activity was digitized at 40 kHz, bandpass filtered from 250 Hz to 8 kHz, and isolated by time-amplitude window discrimination and template matching using a Neural Data Acquisition System (Omniplex, Plexon). Single-unit spike sorting was performed using Off-Line Spike Sorter (OFSS, Plexon) for all behavioural sessions. Principal-component scores were calculated for unsorted waveforms and plotted in a three-dimensional principal-component space; clusters containing similar valid waveforms were manually defined. A group of waveforms were considered to be generated from a single neuron if the waveforms formed a discrete, isolated, cluster in the principal-component space and did not contain a refractory period less than 1 ms, as assessed using auto-correlogram analyses. To avoid analysis of the same neuron recorded on different channels, we computed cross-correlation histograms. If a target neuron presented a peak of activity at a time that the reference neuron fired, only one of the two neurons was considered for further analysis. Spike timestamps were analysed (Neuroexplorer 5, Nex Technologies) to calculate average firing rates and *z*-score transformations of cells depending on behavioural parameters: that is, within and outside freezing episodes. Optical identification of single units was performed as previously described[48]. Briefly, laser light pulses of 100–300 ms duration were used to evoke spiking activity. Short latencies (GAD2$^+$ cells: ≤15 ms; vGluT2$^+$ cells: ≤10 ms) of reliable light-evoked spiking were considered to indicate direct light activation and, thus, allowed for identification of the cell type. To correlate single-unit activity with freezing behaviour, we calculated *z*-scores 2 s before and after onset of freezing during the entire recall session for recordings both of unidentified or of optically identified single units.

Statistics. The experiments were not randomized. No statistical methods were used to predetermine sample size. Data presented in box–whisker plots indicate medians, interquartile range and 5th–95th percentiles. Motion data are presented as s.e.m. range. All other data are presented as means ± s.e.m. Statistical analyses were performed in Graphpad Prism 6.0a or using R. Normality was assessed using Shapiro-Wilk tests. Whenever the normality test failed, non-parametric Mann–Whitney or Wilcoxon signed-rank (for repeated measures) tests were used for pairwise comparisons. Within-subject group analysis of non-parametric data was performed using Friedmann's test with a post-hoc Dunn's multiple comparisons test. Between-subject group analysis of non-parametric data was done with Kruskal–Wallis statistics and a post-hoc Dunn's multiple comparisons test. Variance in normally distributed data sets was analysed with one-way ANOVA and Tukey's or Sidak's post-hoc tests. Significance levels are indicated as follows: $*P < 0.05$; $**P < 0.01$; $***P < 0.001$. See Supplementary Information for statistics table.

51. Franklin, K. B. J. & Paxinos, G. *Atlas of the Mouse Brain* 4th edn (Academic, 2001).

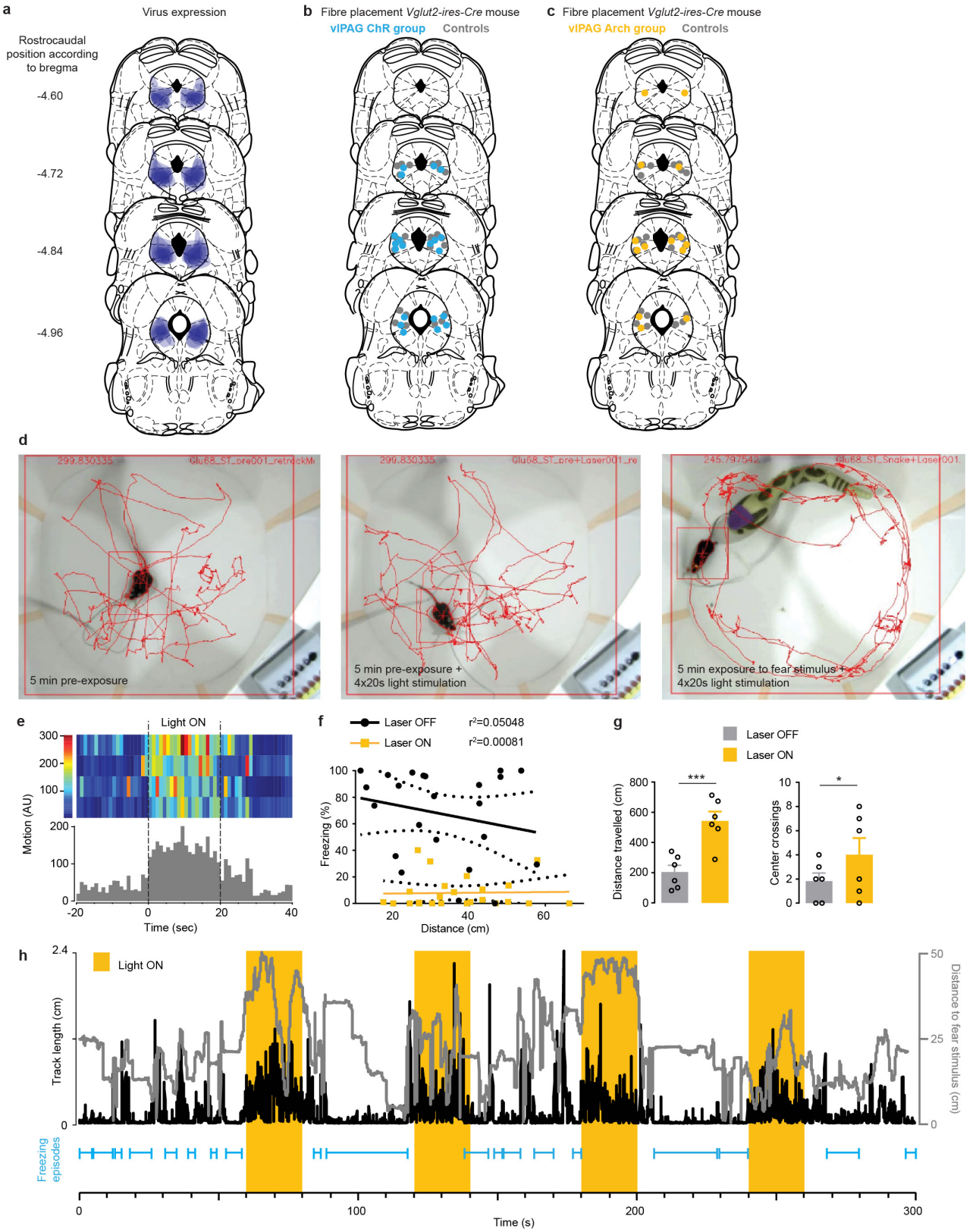

Extended Data Figure 1 | a, Expression of ChR2 throughout vlPAG in consecutive coronal brain sections[51]. **b**, **c**, Fibre placements in *Vglut2-ires-Cre* mice of experimental and control groups. **d**, Supplementary Video stills with superimposed representative movements tracks during the snake open-field test for unconditioned defensive responses. **e**, Colour-coded plot for a mouse's motion before, during and after light-mediated inhibition of vlPAG glutamatergic neurons expressing Arch during a snake open-field test session. **f**, Freezing responses plotted against mouse–snake distance during 'light on' and 'light off' periods showing no linear correlation. **g**, Effects of light-mediated inhibition of vlPAG glutamatergic neurons on anxiety-like behaviour in the open field test with no snake present. Inhibition of vlPAG glutamatergic cells resulted in enhanced track length ($n = 6$ mice, paired two-tailed Student's t-test) and more frequent visits to the centre of the open field ($n = 6$ mice, paired two-tailed Student's t-test). **h**, Example of an entire snake open-field test session, with track length, freezing episodes and mouse–snake distance. Values are means ± s.e.m.

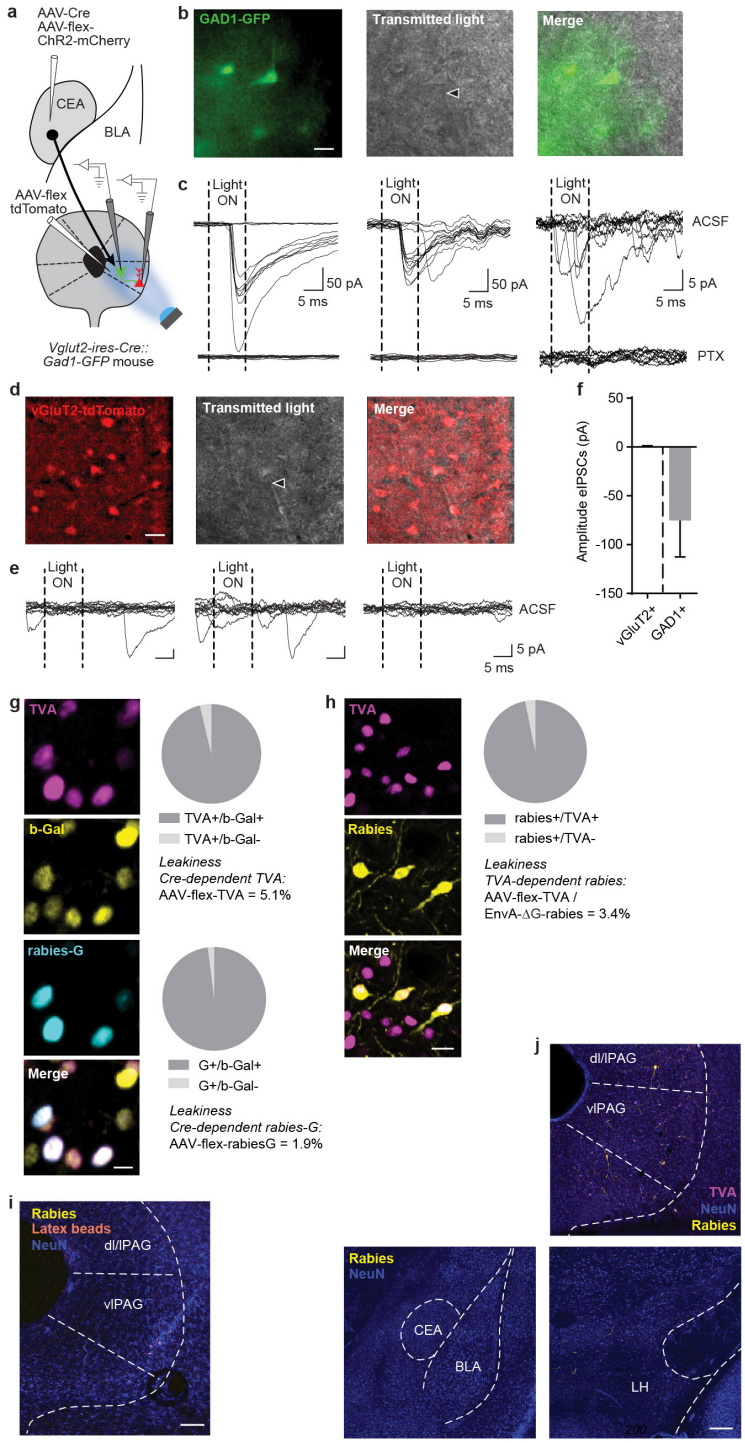

k

Mouse line	Target site	Number of mice	Viruses injected			Starter cells	rabies+ neurons	
			EnvA-ΔG-rabies	AAV-flex-TVA	AAV-flex-G		CEA	HYP
wt	vlPAG	3	+	-	-	0	0	0
wt	vlPAG	3	+	+	+	2.3 ±0.3	0	0

Extended Data Figure 2 | a, *In vitro* slice recordings of functional connectivity between CEA and GABAergic or glutamatergic neurons in vlPAG. **b**, Targeting of fluorescently labelled GAD1$^+$ neurons for whole-cell patch clamp recordings (triangle indicates patch pipette, scale bar, 20 μm). **c**, Example traces of three GAD1$^+$ cells (from three slices of three mice) showing eIPSCs upon light stimulation (10 ms duration) of afferents from the CEA (upper traces), and blockage of eIPSCs by PTX (lower traces). **d**, Targeting of fluorescently labelled vGluT2$^+$ neurons for whole-cell patch clamp recordings (triangle indicates patch pipette; scale bar, 20 μm). **e**, Example traces of three light non-responsive vGluT2$^+$ neurons (from the same three slices as in **c**). **f**, Quantification of eIPSCs amplitudes. **g**, Analysis of specificity of AAV-mediated expression of TVA and rabiesG (scale bar, 10 μm). **h**, Analysis of specificity of TVA-dependent EnvA-ΔG–mCherry–rabies infection (scale bar, 20 μm). **i**, **k**, Lack of EnvA-ΔG–mCherry–rabies infection after injection into wild-type mice (scale bar, 100 μm). **j**, **k**, Leakiness analysis of the combined AAV and EnvA-ΔG–mCherry–rabies tracing system in wild-type mice (scale bar, 200 μm). Values are means ± s.e.m.

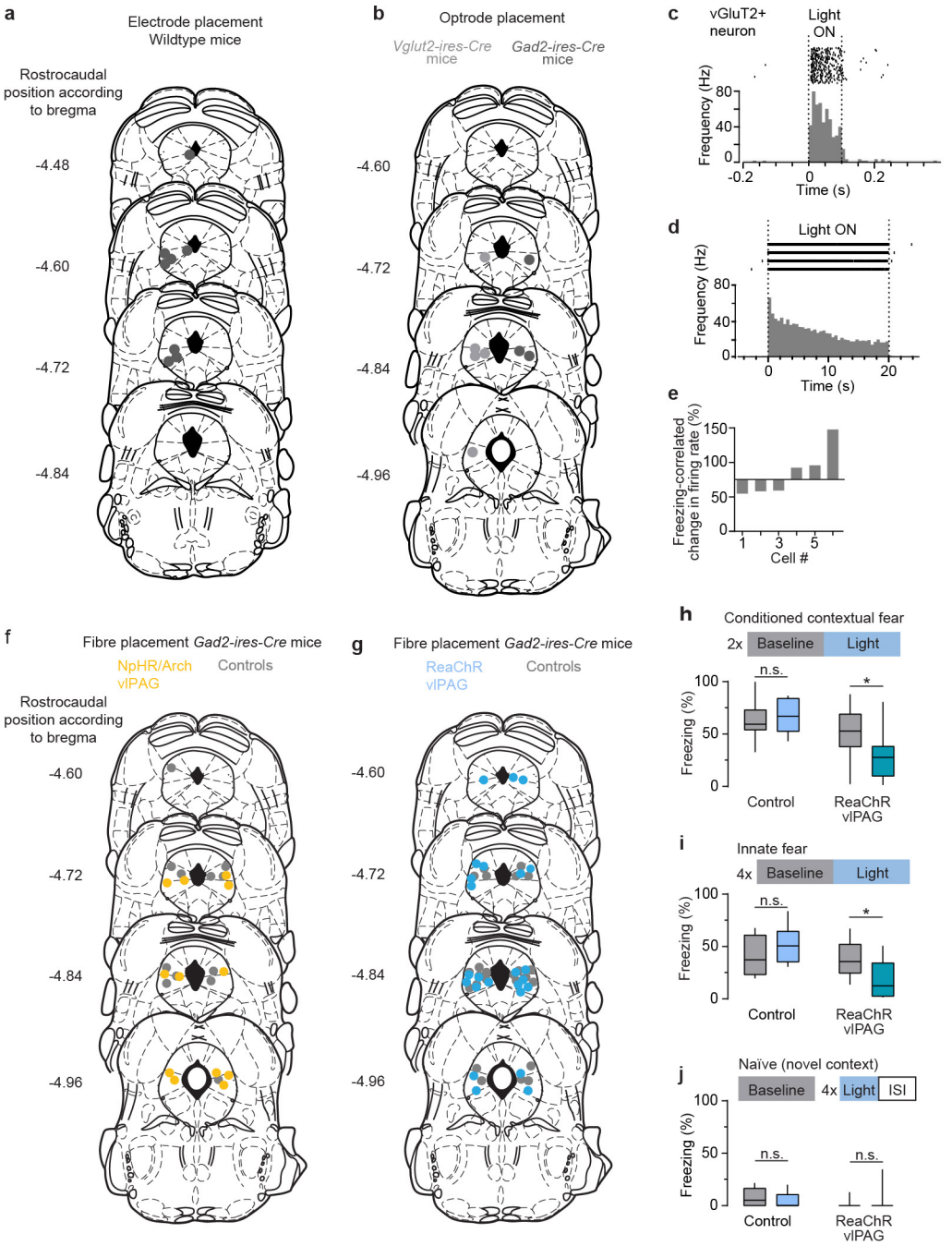

Extended Data Figure 3 | a, Electrode placements for the recordings of unidentified single units. **b**, Placements of optrodes for the recordings of identified neurons. **c**, Raster-frequency plot of an optically identified vlPAG vGluT2$^+$ neuron. **d**, A glutamatergic neuron exhibiting marked optical activation during constant illumination for 20 s. **e**, Identified vGluT2$^+$ neurons ($n = 6$) showed both increased and decreased activity during freezing. **f**, **g**, Fibre placements in *Gad2-ires-Cre* mice expressing inhibitory or excitatory optical actuators. **h**, **i**, Activation of vlPAG GAD2$^+$ neurons resulted in reduced conditioned contextual freezing ($n = 12$ ChR2, $n = 7$ control, paired two-tailed Student's *t*-test) and lower innate freezing levels during the snake open-field test ($n = 10$ ChR2, $n = 8$ control, two-tailed Wilcoxon signed-rank test). **j**, Optical activation of vlPAG GAD2$^+$ neurons had no effect on freezing in naive mice ($n = 8$ ChR2, $n = 8$ control, two-tailed Wilcoxon signed-rank test). Box–whisker plots indicate median, interquartile range, and 5th–95th percentiles of the distribution. $^*P < 0.05$.

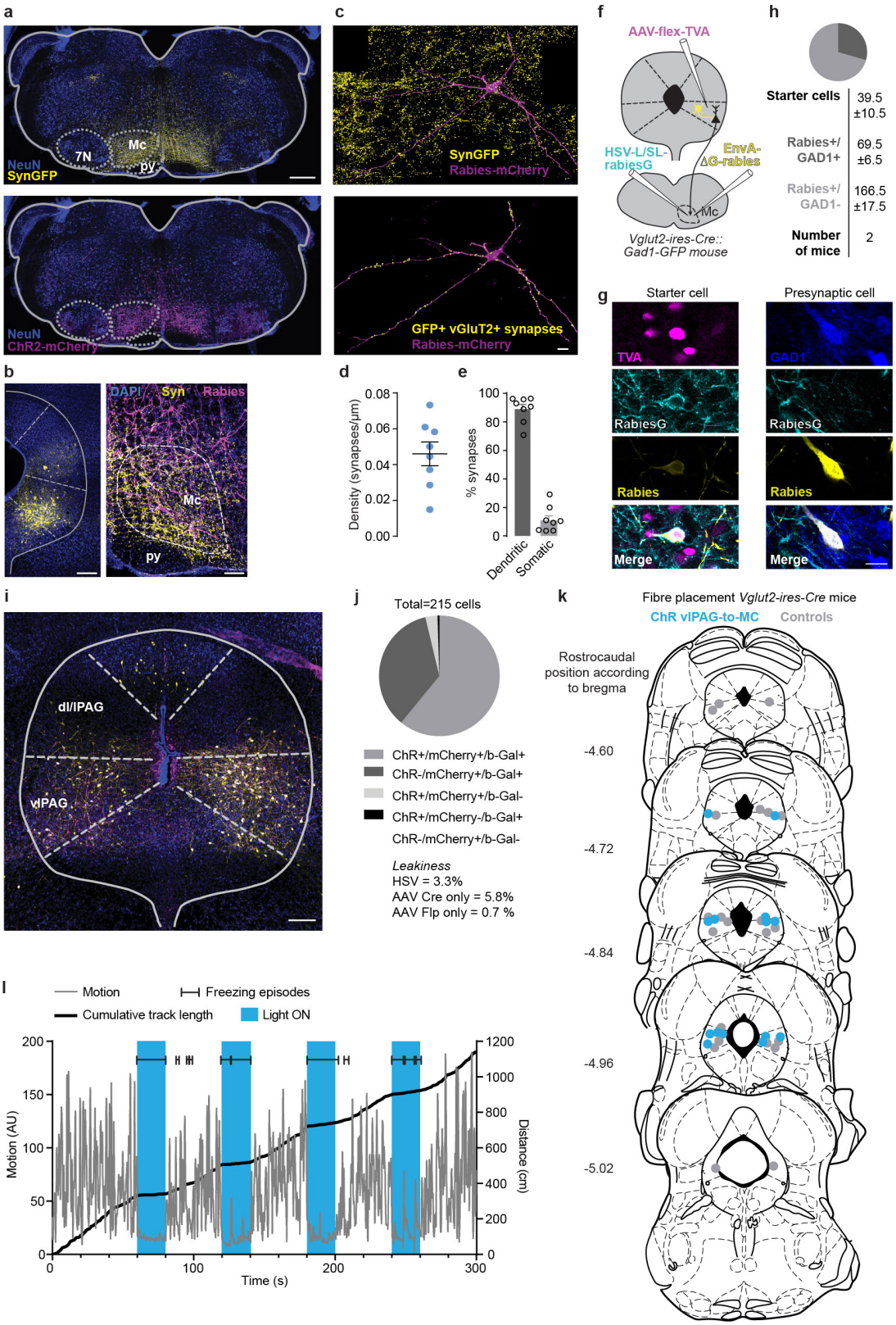

Extended Data Figure 4 | See next page for caption.

Extended Data Figure 4 | a, Projection pattern of glutamatergic vlPAG axonal inputs to the rostral medulla. Terminals of vGluT2$^+$ vlPAG projection neurons were labelled by AAV-mediated expression of GFP fused to presynaptic marker synaptophysin (top; scale bar, 400 μm), and ChR2–mCherry expression was visualized using immunohistochemistry (bottom). **b**, Concomitant AAV-mediated expression of Syn–GFP in vlPAG neurons (left panel, scale bar, 200 μm) labelled presynaptic terminals within Mc (right panel, scale bar, 100 μm). **c**, High-resolution image of a retrogradely traced Mc pre-motor neuron (rabies–mCherry) and SynGFP$^+$ vlPAG inputs (top), and visualization of identified glutamatergic synaptic contacts (bottom; scale bar, 10 μm). **d**, **e**, Density of vGluT2$^+$ vlPAG synaptic inputs to pre-motor neurons in Mc ($n = 8$ cells from three mice), and quantification of their distribution between the dendritic or somatic compartment. **f**, Intersectional EnvA-ΔG–mCherry–rabies tracing approach to identify local GABAergic inputs to vlPAG-to-Mc-projecting glutamatergic cells. **g**, TVA-, rabiesG- and EnvA-ΔG–mCherry–rabies triple-positive cells were identified as starter cells (left panels), while GAD1 and EnvA-ΔG–mCherry–rabies double positive cells indicated presynaptic GABAergic neurons (right panels; scale bar, 20 μm). **h**, Quantification of GAD1$^+$ or GAD1$^-$ presynaptic cells ($n = 2$ mice; dark grey, rabies$^+$/GAD1$^+$; light grey, rabies$^+$/GAD1$^-$). **i**, Example picture of glutamatergic vlPAG neurons retrogradely traced from the Mc, expressing ChR2 in presence of Cre and Flp recombinase (scale bar, 200 μm). **j**, Analysis of viral efficacy and leakiness. Overlaps of ChR delivered by AAV-Cre^{ON}Flp^{ON}-ChR2, HSV-delivered Cre-dependent Flp–mCherry and Cre-dependent β-Gal were quantified in *Vglut2::LacZ* reporter mice. **k**, Fibre placement in *Vglut2-ires-Cre* mice expressing ChR2 in glutamatergic vlPAG-to-Mc projection neurons. **l**, Example of an entire session of light activation of glutamatergic vlPAG-to-Mc projection neurons, with the mouse's motion, cumulative track length and light-induced freezing bouts. Values are means ± s.e.m.

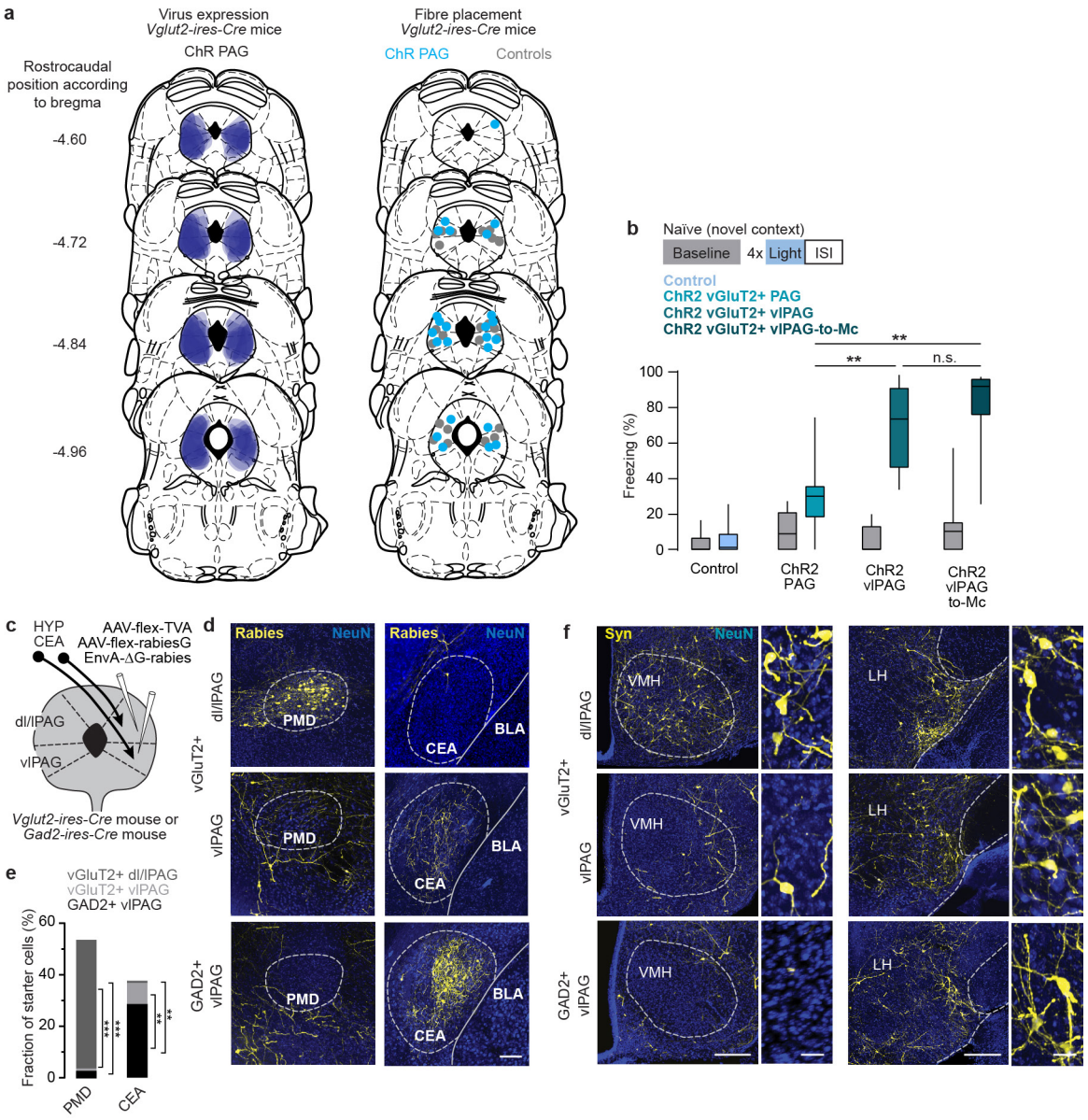

g

Target site	Target cell type	Number of mice	Number of starter cells	Number of presynaptic cells							
				CEA	DM	AHM	VMH	PH	PLH	LH	PMD
dl/lPAG	vGlut2+	3	509 ±154	5 ±3	30 ±14.6	53.33 ±28.7	86.67 ±35.3	71.33 ±30.7	60 ±26.9	77 ±33.1	251.7 ±77.4
vlPAG	vGlut2+	3	695 ±135	58 ±27	12.67 ±7.3	38 ±9.5	11.67 ±2.7	36.33 ±5.8	83 ±19.9	81.67 ±17.9	6.333 ±1.7
vlPAG	GAD2+	4	265 ±105	94.3* ±53.2	3.7 ±2.8	7 ±3.7	1.5 ±0.9	3.75 ±3.1	20.75 ±7.4	22.25 ±9.5	6.25 ±3.1

*one outlier (=271) was removed (Grubb's test, alpha = 0.01)

Extended Data Figure 5 | a, Expression of ChR2 throughout PAG in consecutive coronal brain sections (left), and fibre placements in *Vglut2-ires-Cre* mice of experimental and control groups (right). **b**, Light-evoked effect on freezing behaviour induced by activation of different glutamatergic subpopulations of PAG neurons in naive animals ($n = 12$ PAG, $n = 10$ vlPAG, $n = 7$ vlPAG-to-Mc, Kruskal–Wallis test, $P < 0.001$, Dunn's multiple comparison post-hoc test). **c**, EnvA-ΔG–mCherry–rabies-mediated, Cre-dependent monosynaptic retrograde tracing of inputs to GAD2$^+$ and vGluT2$^+$ neurons in the vlPAG and dl/lPAG. **d**, Rabies-mediated labelling of presynaptic neurons within PMD (left panels) and CEA (right panels) of *Gad2-ires-Cre* and *Vglut2-ires-Cre* mice (scale bar, 100 μm). **e**, Statistical analysis reveals differential input to vGluT2$^+$ ($n = 3$ mice for each vlPAG and dl/lPAG) and GAD2$^+$ ($n = 4$ mice) neurons within vlPAG or dl/lPAG. While CEA preferentially targets GAD2$^+$ neurons of the vlPAG (1×3 ANOVA, $F_{(2,6)} = 21.67$, $P < 0.01$, Tukey's post-hoc test), vGluT2$^+$ neurons of the dl/lPAG receive stronger inputs from PMD (1×3 ANOVA, $F_{(2,7)} = 287$, $P < 0.0001$, Tukey's post-hoc test). **f**, Cell-type-specific monosynaptic rabies tracing of VMH and LH inputs to vGluT2$^+$ neurons in the dl/lPAG, vlPAG and vlPAG GAD2$^+$ neurons (scale bars in overview, 200 μm; in zoom-in, 25 μm). **g**, Quantification of starter cells in the PAG and presynaptic cells in CEA and hypothalamic subregions. Boxes indicate median and 25th–75th percentiles of the distribution. $^{**}P < 0.01$; $^{***}P < 0.001$.

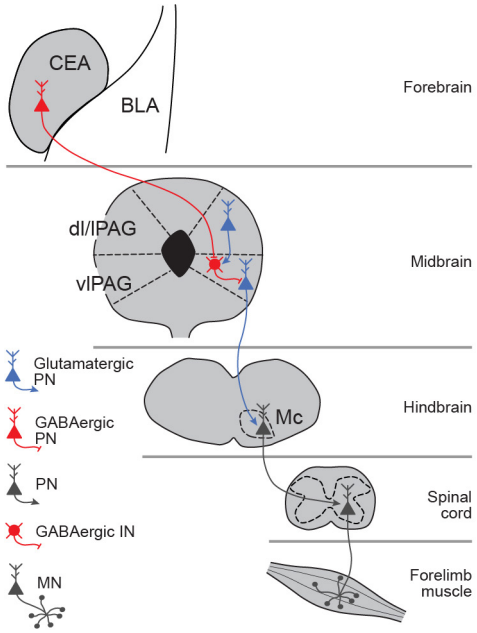

Extended Data Figure 6 | Schematic representation of the freezing pathway. PN, projection neuron; IN, interneuron; MN, motor neuron.